Agricultural and Forest Meteorology 220 (2016) 50–68

Contents lists available at ScienceDirect

Agricultural and Forest Meteorology

journal homepage: www.elsevier.com/locate/agrformet

Response and biophysical regulation of carbon dioxide fluxes to climate variability and anomaly in contrasting ecosystems in northwestern Ohio, USA

Housen Chu[a,b,*], Jiquan Chen[a,c,d], Johan F. Gottgens[a], Ankur R. Desai[e], Zutao Ouyang[a,c,d], Song S. Qian[a]

[a] Department of Environmental Sciences, University of Toledo, 2801W. Bancroft, Toledo, OH 43606, USA
[b] Department of Environmental Sciences, Policy, and Management, University of California, Berkeley, 130, Mulford Hall, Berkeley, CA 94720, USA
[c] Center for Global Change and Earth Observations, Michigan State University, 218 Manly Miles Building, 1405 S. Harrison Road, East Lansing, MI 48823, USA
[d] Department of Geography, Geography Building, 673 Auditorium Rd, East Lansing, MI 48824, USA
[e] Department of Atmospheric and Oceanic Sciences, University of Wisconsin-Madison, 1225W Dayton St, Madison, WI 53706, USA

ARTICLE INFO

Article history:
Received 3 April 2015
Received in revised form 5 January 2016
Accepted 8 January 2016

Keywords:
Functional change
Interannual variability
Net ecosystem exchange
Climate anomaly

ABSTRACT

Recent climate variability and anomaly in the Great Lakes region provided a valuable opportunity in examining the response and regulation of ecosystem carbon cycling across different ecosystems. A simple Bayesian hierarchical model was developed and fitted against three-year (2011–2013) net ecosystem CO_2 exchange (F_{CO_2}) data observed at three eddy-covariance sites (i.e., a deciduous woodland, a cropland, and a marsh) in northwestern Ohio. The model was designed to partition the variation of gross ecosystem production (GEP), ecosystem respiration (ER) and F_{CO_2} that resulted directly from the short-term environmental forcing (i.e., direct effect) and indirectly from the changes of ecosystem functional traits (e.g., structural, physiological, and phenological traits) (i.e., indirect effect). Interannual variation of F_{CO_2} was mainly driven by indirect effects, accounting for 54%, 89%, and 86% of the interannual variation at the woodland, cropland, and marsh sites, respectively. On the other hand, direct climatic effects accounted for 33% of interannual F_{CO_2} variation at the woodland site and became irrelevant (<10%) at the cropland and marsh sites. In general, annual GEP and ER at each site tended to co-vary and dampen the interannual variability in F_{CO_2}. Yet, year-to-year changes of GEP and ER were not spatially synchronous, suggesting that the ecosystem's response to climate was strongly site-specific in terms of the annual net CO_2 uptake. Future research should focus on the disparate response among ecosystems and develop a suitable framework to examine the mechanisms that drive differences in closely co-located ecosystems.

1. Introduction

Net ecosystem CO_2 exchange (F_{CO_2}), which is the balance of two large and opposite carbon fluxes-gross ecosystem production (GEP) and ecosystem respiration (ER)—has been studied across a range of spatial and temporal scales in recent decades to understand how climatic variability and disturbance regulate the regional-to-global carbon balance (Baldocchi, 2014; Braswell et al., 1997; Melillo et al., 2014; Yi et al., 2010). Environmental drivers, such as solar radiation, temperature, and air/soil moisture, are generally accepted as the major factors regulating the variation of CO_2 fluxes (i.e., F_{CO_2}, GEP, ER) at the hourly to synoptic (multi-daily) scales (Baldocchi et al., 2001; Baldocchi, 2008; Stoy et al., 2005). On the other hand, the response of CO_2 fluxes to climatic variability becomes more complex at a longer scale (e.g., seasonal to interannual) and often involves indirect effects (i.e., prolonged, muted, and lagged responses) through altering the biotic characteristics (Barr et al., 2009; Humphreys and Lafleur, 2011; Richardson et al., 2010; Stoy et al., 2005). The interaction of direct and indirect effects is of great importance because the similarity or difference in their response magnitudes/directions to climatic variability may reveal the potential resilience or vulnerability of ecosystem carbon cycling to prospective climate change (Cox et al., 2000; Heimann and Reichstein, 2008; Luo et al., 2009).

Different statistical frameworks, such as the homogeneity-of-slopes model (e.g., Hui et al., 2003; McVeigh et al., 2014; Polley et al.,

* Corresponding author at: University of California, Berkeley, Department of Environmental Sciences, Policy, and Management, 130 Mulford Hall, Berkeley, CA 94720, USA.
E-mail addresses: hchu@berkeley.edu, chu.housen@gmail.com (H. Chu).

http://dx.doi.org/10.1016/j.agrformet.2016.01.008
0168-1923/

2008; Teklemariam et al., 2010) and the cross-year model simulation (e.g., Richardson et al., 2007; Shao et al., 2014; Wu et al., 2012), have been adopted to disentangle the direct/indirect effects. In general, these approaches took advantage of our current understanding of environmental forcing on the short-term variability of CO_2 fluxes. They structured the statistical models explicitly to incorporate all relevant short-term environmental drivers (e.g., radiation, temperature, moisture) and allowed the model parameters to vary across a longer time span (e.g., yearly, in most cases). Once the models were fitted, the variation of CO_2 fluxes (e.g., among years) was then partitioned into the effects of environmental drivers (i.e., direct effect) and model parameters (i.e., indirect effect). The changes of model parameters were interpreted as "functional changes" (Hui et al., 2003), which comprised of all effects that were unexplained by direct and instantaneous environmental forcing.

Potentially, the functional changes may result from the changes of plant phenology (Richardson et al., 2009, 2010), physiological characteristics (Luo et al., 2001; Sala et al., 2010), canopy structure (Barr et al., 2004; Humphreys and Lafleur, 2011), soil microbial community (Sowerby et al., 2005), substrate availability (DeForest et al., 2009), or the interplay of autotrophic and heterotrophic respiration (DeForest et al., 2006; Xu et al., 2011). Studies showed that the indirect effects often played a dominant role in driving interannual F_{CO_2} variability (Shao et al., 2015). In some cases, the indirect effects explained up to ~70–80% of the interannual variability of CO_2 fluxes (Shao et al., 2014; Wu et al., 2012). However, prior studies have not been applied to a collection of co-located sites experiencing a set of extreme climate anomalies, where the expectation would be similar responses given similar climate mean state and geographic distance.

Recent research also highlighted the importance of rare but extreme weather events (e.g., heat/cold wave, rain storm, severe drought) for their disproportional influence on ecosystem carbon cycling (Ciais et al., 2005; Shi et al., 2014; Wu et al., 2012; Xiao et al., 2010). Climatic anomalies and extremes posed instantaneous effects on ecosystem carbon cycling by altering environmental conditions (i.e., temperature, moisture). More importantly, these events may alter the phenological, physiological, and structural traits of ecosystems, which then translate into indirect effects that last much longer than the duration of climatic anomalies and extremes (Ciais et al., 2005; Teklemariam et al., 2010; Thibault and Brown, 2008). These prolonged or lagged effects often resulted in more influence on carbon cycling than the short-term direct effects (Ciais et al., 2005; Desai, 2014; Thibault and Brown, 2008).

Most recently, severe weather and climate anomalies have been increasingly observed in United States (Karl et al., 2012; Wuebbles et al., 2014). In the Great Lakes region, the recent records included the earliest false spring of the century (2012), heat waves (2011, 2012), summer cool spells (2013), and record-breaking high precipitation (2011) (Ault et al., 2013; Chu et al., 2015; Karl et al., 2012). These anomalies triggered drastic year-to-year variation in plant phenology across the region and caused severe damages to crop and fruit production (Ault et al., 2013; Knudson, 2012). Our previous study found that a Lake Erie coastal marsh turned from a net carbon sink to a net carbon source recently in the past years (Chu et al., 2015). However, it remains unclear whether the influence was ecosystem-specific or region-wide, and to what extent the influence was caused by direct and indirect effects.

Here, we aimed to examine and compare the effects of recent climatic variability and anomalies on interannual variability of CO_2 fluxes at different ecosystems in the region. Specifically, we targeted the two largest carbon fluxes (GEP and ER) and their balance $-F_{CO_2}$. We asked the following questions. (1) Do spatially co-located but functionally different ecosystems respond similarly in magnitude and direction to climate variability and anomalies in terms of CO_2 fluxes? (2) What biophysical factors most influence how ecosystem CO_2 fluxes (GEP, ER, and F_{CO_2}) respond to recent climate variability and anomalies? (3) To what extent can the response of GEP, ER, and F_{CO_2} be explained by the direct and indirect effects at different ecosystems, respectively? Specifically, do these direct and indirect effects function synergistically (++) or antagonistically (+−) to the climate variability and anomalies?

2. Materials and methods

2.1. Experiment design

We adopted a similar cross-year model simulation approach as in Richardson et al. (2007) and Wu et al. (2012). We targeted the three most prevalent ecosystem types (i.e., agriculture, forest, and wetland) in the study region—northwestern Ohio, USA. A Bayesian hierarchical model was developed and the model parameters were estimated using the Markov Chain Monte Carlo (MCMC) technique. The models were fitted against three-year (2011–2013) F_{CO_2} data observed at three eddy-covariance sites in the region (Table 1).

We designed the model to incorporate the most relevant short-term (hourly-synoptic) environmental forcing on GEP and ER (i.e., solar radiation, temperature, air/soil moisture) and allowed model parameters to vary through the seasons and over years. Once the models were fitted, we ran a series of Monte Carlo simulations ($N = 1000$) at each half-hourly time step through a yearly time span (17,520 steps) by using model parameters from each year (2011–2013) with environmental drivers from each year (2011–2013). The cross-year simulation generated nine different scenarios of the parameter-driver combinations (e.g., 2011 driver × 2011 parameter, 2011 driver × 2012 parameter...). The simulated half-hourly GEP, ER, and F_{CO_2} were then integrated locally (i.e., every eight days) and annually.

Following Richardson et al. (2007), we adopted analysis of variance (ANOVA) to partition the variation of local and annual integrals

Table 1
Summary of the site location and vegetation types in the study.

Site	Oak Openings preserve (US-Oho)	Curtice Walter–Berger cropland (US-CRT)	Winous Point north marsh (US-WPT)
Location	N41°33′16.98″ W83°50′36.76″	N41°37′42.31″ W83°20′43.18″	N41°27′51.28″ W82°59′45.02″
Vegetation type	Deciduous broadleaf forest (~70-year)	Conventional rain-fed cropland	Freshwater coastal marsh
Dominant species	*Quercus rubra*, *Q. alba*, *Q. velutina*, *Acer rubrum*	*Glycine max*, *Triticum spp.*	*Nymphaea odorata*, *Nelumbo lutea*, *Typha angustifolia*, *Hibiscus moscheutos*
Soil type	Sandy mixed and mesic	Silty clay	Hydric
Groundwater level	0.3–3 m belowground	0.3–3 m belowground	0.2–1 m aboveground
Soil water content	17–25%	25–65%	Saturated
Reference	Noormets et al. (2008b) and Xie et al. (2014)	Chu et al. (2014)	Chu et al. (2014, 2015)

from the nine different simulation scenarios into the effects of parameter years (i.e., indirect effect), driver years (i.e., direct effect), their interactions (if significant), and residual errors. Instead of hypothesis testing, we adopted ANOVA in order to interpret to what extent the simulated interannual GEP/ER/F_{CO_2} variability resulted from the instantaneous/direct response to the short-term environmental forcing. On the other hand, interannual variability resulting from the varying parameters over the years was interpreted as the lagged/prolonged response from altering the phenological, structural, or physiological traits of ecosystems. Herein, we treated the nine scenario's composite average as a conceptual baseline while presenting interannual variation of simulated GEP, ER and F_{CO_2}. Unless specified, we always reported parameter estimations and simulations in terms of medians along with 95% quantile intervals (2.5%, 97.5%) in the following sections.

2.2. Site and date description

The three flux tower sites, which include a 70-year-old deciduous woodland in the Oak Openings Preserve (AmeriFlux: US-Oho), a freshwater marsh at the Winous Point Marsh Conservancy (US-WPT), and a conventional cropland (US-CRT) are located 30–50 km apart in northwestern Ohio (Table 1). The climate conditions are similar at the three sites with a long-term regional mean air temperature of ~10.0 °C and annual precipitation of ~897 mm (Chu et al., 2014). The mixed woodland is dominated by red oak (*Quercus rubra*), white oak (*Quercus alba*), black oak (*Quercus velutina*), and red maple (*Acer rubrum*). The freshwater marsh is permanently inundated and covered with a mix of narrow-leaved cattail (*Typha angustifolia*) and water lily (*Nymphaea odorata*) interspersed with areas of open water. The cropland site is rain-fed and no irrigation is applied. The cultivation practices include minimum tillage and both insect and weed control. During the three year study period, the cropland was planted with soybean (*Glycine max*) in 2011 (DOY 162–296) and 2012 (DOY 141–275). Winter wheat (*Triticum spp.*) was planted after the soybean harvest in 2012 and was harvested on DOY 197 in 2013. Detailed site information can be found in Chu et al. (2014, 2015), Noormets et al. (2008b), and Xie et al. (2014).

Micrometeorological variables were measured at all the sites, including photosynthetically active radiation (PAR), air temperature (T_a), vapor pressure deficit (VPD), precipitation (PP), soil temperature (T_g), groundwater level, and volumetric soil water content (VWC). Regional long-term meteorological data (i.e., T_a and PP) were obtained through the National Climatic Data Center of the National Oceanic and Atmospheric Administration, USA. The three-year (2011–2013) regional climate was summarized as being extremely warm in 2012 and having high precipitation in 2011 (Fig. A1) (Chu et al., 2015). Additionally, there were several warm spells in 2011 and 2012 and cool spells in the summer of 2013.

The eddy covariance method was applied to quantify F_{CO_2} at all the sites following the same workflow described in Chu et al. (2014). In total, 42%, 73% and 61% of F_{CO_2} passed the quality control checks at the woodland, marsh, and cropland sites, respectively. The quality-controlled and non-gap-filled F_{CO_2} was used for further model parameterization. In addition, we applied the marginal distribution sampling (MDS) method to fill the F_{CO_2} gaps (Reichstein et al., 2005). The MDS method was selected for its consistently good gap-filling performance across sites (Moffat et al., 2007; Papale et al., 2006). Thus, we adopted the MDS-filled annual F_{CO_2} as a reference estimate in comparison with those from the model simulations. Details of the gap-filling procedures and uncertainty estimations can be found in our previous study (Chu et al., 2014).

We adopted enhanced vegetation index (EVI) as a land surface vegetation index to provide information of seasonal vegetation dynamics (e.g., canopy coverage, greenness, and biomass) (Morisette et al., 2008). Eight-day EVI was calculated from the reflectance (MOD09A1) of the Moderate Resolution Imaging Spectroradiometer (MODIS) instrument from the Land Process Distributed Active Archive Center, US Geological Survey, USA. The target spatial coverage was 500 × 500 m^2 at the marsh and cropland sites and 2500 × 2500 m^2 at the woodland site, respectively.

2.3. Model description

The F_{CO_2} was modeled at the half-hourly time step. We assumed F_{CO_2} followed a distribution, where the mean ($\mu_{F_{CO_2}}$) can be modeled as the difference of GEP and ER. The standard deviation ($\sigma_{F_{CO_2}}$) can be modeled as a function of PAR to incorporate the heteroscedasticicity (Richardson et al., 2006), where w_1 and w_2 were the empirical coefficients:

$$F_{CO_2} \sim N(\mu_{FCO_2}, \sigma^2_{FCO_2}) \tag{1}$$

$$\mu_{F_{CO_2}} = ER - I(PAR - 10) \times GEP; I(x) = \begin{cases} 0, & x \le 0 \\ 1, & x > 0 \end{cases} \tag{2}$$

$$\sigma_{F_{CO_2}} = w_1 + w_2 \times PAR; w_i \sim N\left(\mu_{wi}, \sigma^2_{wi}\right) \tag{3}$$

where the step function $I(x)$ was used for discriminating the daytime/nighttime data (PAR > 10 μmol m^{-2} s^{-1} for daytime) such that the model could be estimated by using the daytime and nighttime data together. Positive F_{CO_2} indicated a net flux from the ecosystem to the atmosphere. GEP and ER were both set to be positive.

The Arrhenius equation (Lloyd and Taylor, 1994) and Michaelis–Menten light response equation (Falge et al., 2001) were adopted as the basic models for ER and GEP, respectively. In addition, two exponential decaying functions were introduced to account for VPD limitation on GEP and VWC limitation on ER (Lasslop et al., 2010; Noormets et al., 2008a):

$$ER = R_{ref} \times \exp\left[E_0\left(\frac{1}{T_{ref} - T_0} - \frac{1}{T_a - T_0}\right)\right] \times \varphi(VWC) \tag{4}$$

$$GEP = A_{\max} \times \left(\frac{PAR}{PAR + K_m}\right) \times \varphi(VPD) \tag{5}$$

$$\varphi(VWC) = \begin{cases} 1, & VWC^* \ge VWC_0 \\ \exp[-k_{VWC}(VWC_0 - VWC^*)], & VWC^* < VWC_0 \end{cases} \tag{6}$$

$$\varphi(VPD) = \begin{cases} 1, & VPD^* \le VPD_0 \\ \exp[-k_{VPD}(VPD^* - VPD_0)], & VPD^* > VPD_0 \end{cases} \tag{7}$$

where VPD* and VWC* were the normalized VPD (0–1) and VWC (0–1) against the observed full ranges. R_{ref} (μmol CO_2 m^{-2} s^{-1}) was the base respiration at the reference temperature (T_{ref}, set as 10 °C), E_0 (°C) was the temperature sensitivity, T_0 was set to be −46.02 °C, A_{max} (μmol CO_2 m^{-2} s^{-1}) was the maximum ecosystem CO_2 uptake rate at light saturation, and K_m (μmol quanta m^{-2} s^{-1}) was the half-saturation quantum flux level of the GEP light response curve. k_{VPD} and k_{VWC} represented the sensitivities for VPD and VWC limitation whereas VPD_0 and VWC_0 were the thresholds for VPD and VWC limitation.

In the preliminary tests, we found that certain parameters (e.g., A_{max}-K_m-k_{VPD}-VPD_0) tended to co-vary. If all these parameters were allowed to vary through the time series without proper constraints, model parameterization either did not converge or led to unreasonable estimations when it did. Thus, we reduced the model structures based on current knowledge about these parameters' temporal characteristics and set different parameters to vary at specific time steps (Appendix A) (Bloom and Williams, 2015; Shao et al., 2014). R_{ref} and A_{max} were allowed to vary every day within each year and among years while the rest (e.g., E_0, K_m...) were set

Table 2
Medians and 95% quantile intervals (2.5%, 97.5%) of the posterior distributions and the lower and upper bounds [lower, upper] of the uniform prior distributions of model parameters at the woodland, marsh, and cropland sites[a]

Parameter	Posterior			Prior
	2011	2012	2013	Hyper parameter
Woodland site				
E_0	232 (203,261)	58 (50,77)	52 (50,58)	[50,400]
K_m	1330 (12,371,424)	1762 (1644,1896)	1822 (1666,1968)	[100,2000]
k_{VWC}		0.67 (0.46,0.88)		[0,10]
VWC_0		0.55 (0.47,0.63)		[0,10]
k_{VPD}		0.82 (0.77,0.87)		[0,10]
VPD_0		0.18 (0.17,0.20)		[0,10]
Marsh site				
E_0	178 (160,196)	86 (68,105)	91 (71,109)	[50,400]
K_m	662 (607,718)	690 (619,760)	430 (383,483)	[100,2000]
k_{VWC}		n.a.		[0,10]
VWC_0		n.a.		[0,10]
k_{VPD}		0.42 (0.15,0.76)		[0,10]
VPD_0		0.45 (0.23,0.53)		[0,10]
Cropland site				
E_0	205 (181,229)	186 (162,210)	76 (55,102)[b]	[50,400]
K_m	1316 (1237,1391)	1184 (1111,1246)	1533 (1459,1612)[b]	[100,2000]
k_{VWC}	0.78 (0.09,8.30)[c]		0.91 (0.29,8.63)[b]	[0,10]
VWC_0	0.32 (0.01,0.74)[c]		0.76 (0.04,0.92)[b]	[0,10]
k_{VPD}	1.23 (1.17,1.29)[c]		0.89 (0.79,0.98)[b]	[0,10]
VPD_0	0.09 (0.07,0.10)[c]		0.06 (0.03,0.07)[b]	[0,10]

[a] E_0, temperature sensitivity (°C); K_m, half-saturation quantum flux level of the GEP light response curve (μmol quanta m^{-2} s^{-1}); k_{VPD}, sensitivity for vapor pressure deficit (VPD) limitation; k_{VWC}, sensitivity for soil water content (VWC) limitation; VPD_0, threshold for VPD limitation; VWC_0, thresholds for VWC limitation; n.a., not available.
[b] For wheat period (September 2012–2013).
[c] For soybean period (2011–September 2012).

to only vary among years (i.e., yearly parameter). Furthermore, we adopted the phenology model in Gu et al. (2009) to describe the seasonal dynamics of R_{ref} and A_{max}, where R_{ref} and A_{max} at each daily step were modeled as functions of the day of year (DOY) (i.e., $\mu A_{max}(t)$, $\mu_{Rref}(t)$). Additionally, the standard deviations (i.e., σA_{max}, σ_{Rref}) were introduced so that R_{ref} and A_{max} can be fine-tuned at each daily step to mimic the multi-day variation that superimposed the seasonality:

$$R_{ref}(t) \sim N\left(\mu_{Rref}(t), \sigma^2_{Rref}\right) \quad (8)$$

$$A_{\max}(t) \sim N\left(\mu_{A\max}(t), \sigma^2_{A\max}\right) \quad (9)$$

$$\mu_x(t) = y_{0.x} + \frac{a_{1.x}}{\left[1+\exp\left(-\frac{t-t_{1.x}}{b_{1.x}}\right)\right]^{c_{1.x}}} - \frac{a_{2.x}}{\left[1+\exp\left(-\frac{t-t_{2.x}}{b_{2.x}}\right)\right]^{c_{2.x}}} \quad (10)$$

where t represented the DOY, the first term (y_0) on the right hand side of Eq. (10) represented the baseline R_{ref} or A_{max} of the year and the second and third terms reflected the spring development and fall recession phases of R_{ref} or A_{max}. y_0, a_1, a_2, b_1, b_2, c_1, c_2, t_1, and t_2 were empirical parameters that were associated with either the full ranges of R_{ref} or A_{max} (y_0, a_1, a_2) or the duration/timing of the transition periods (b_1, b_2, c_1, c_2, t_1, t_2). Once the models were fitted, a series of ensemble phenological characteristics, such as the annual assimilation/respiration potentials (i.e., annual integrals), active and peak assimilation/respiration periods, can be calculated from the model coefficients (Table A1; Appendix A) (Gu et al., 2009). While fitting the models, we set all the empirical parameters in Eq. (10) to vary among years in representing the interannual variation.

In our preliminary tests, we also found that the yearly estimates of k_{VWC}, VWC_0, k_{VPD}, and VPD_0 were similar among years. Thus, we further reduced the model structures by treating them as universal parameters (i.e., one set of parameters for three years) similar to other previous studies (e.g., Richardson et al., 2007; Shao et al., 2014). For each yearly parameter, we assumed that the parameters were linked among years (i.e., exchangeability) and the linkage could be described by a higher level distribution (i.e., hierarchical model):

$$\theta_{jl} \sim N\left(\mu_{\theta j}, \sigma^2_{\theta j}\right); \quad \theta_{jl} \in [L_{\theta j}, U_{\theta j}] \quad (11)$$

where θ_{jl} was a yearly estimate of parameter θ_j (e.g., E_0, K_m, y_0, a_1, a_2, b_1, b_2…) at the year l (2011–2013), $\mu_{\theta j}$ and $\sigma_{\theta j}$ were the mean and standard deviation of the higher level distribution from which θ_{jl} was drawn (i.e., hyper parameters). A uniform prior was adopted for each hyper parameter (i.e., $\mu_{\theta j}$, $\sigma_{\theta j}$) bounded within an acceptable range based on literature survey (Table 2; Tables A2–A4) (Zobitz et al., 2011). Also, each yearly parameter was constrained by the lower ($L_{\theta j}$) and upper ($U_{\theta j}$) bounds.

While fitting the model, we estimated all the parameters in Eqs. (1)–(11) together with the entire three-year dataset. For the cropland site, the winter-spring wheat cover at the cropland had two higher assimilation periods (October–November 2012 and May–June 2013) that were separated by the snow-covered period in winter. Thus, an additional set of model parameters was introduced specifically for this winter-wheat period (September–December 2012) in order to adequately capture the bimodal seasonality of A_{max} in 2012.

The GEP and ER models are admittedly semi-empirical. However, as the models were fine-tuned to incorporate the major short-term environmental drivers (e.g., PAR/VPD on GEP, T_a/VWC on ER) of these ecosystems (Chu et al., 2014; Noormets et al., 2008b; Ouyang et al., 2014), the A_{max} and R_{ref} represented the potential GEP and baseline ER after eliminating the short-term dynamics of environmental forcing. We did not use site-specific management factors (e.g., agricultural practice at the cropland, groundwater level at the marsh) in order to keep the model structures and thus variance partition comparable among sites. Herein, these parameters were interpreted as estimates of ecosystem functional traits that were associated with GEP and ER (i.e., functional parameter) (Wu et al., 2012). For example, A_{max} was addressed to be often associated with ecosystem structural (e.g., leaf area index) and physiological (e.g., leaf photosynthesis capacity, nitrogen content)

characteristics (Cook et al., 2004; Ollinger et al., 2008). R_{ref} was often associated with the substrate quality/quantity and microbial composition/activity (Carbone et al., 2008; Cook et al., 2004; Jarvis et al., 2007).

2.4. Model parameterization and model error assessment

All statistical tests and model estimations were conducted in the R platform (R Development Core Team, 2014, version 3.1.1). Bayesian hierarchical models were carried out using the JAGS software (Just Another Gibbs Sampler, version 3.4.0) (Plummer, 2003), which was activated through the "rjags" package. The "dclone" and "snow" packages were used for parallel computation of six chains starting randomly within the prior ranges (Solymos, 2010; Tierney et al., 2009). The Gelman–Rubin convergence was checked by using the "coda" package (Brooks and Gelman, 1998; Plummer et al., 2006). The chains usually converged after less than 15,000–17,000 iterations. After convergence, we ran an updating stage of 5000 iterations, and a final burn-in stage of 3000 iterations. Finally, we kept 1000 parameter sets for following simulations by thinning the last 3000 iterations from all of the six chains (i.e., 167 per chain) to eliminate the autocorrelation of estimates among iterations.

Once the models were fitted, we examined the model performance via a series of inter-comparison between the predicted F_{CO_2} ($F_{CO_2\cdot model}$) and observed/gap-filled F_{CO_2} ($F_{CO_2\cdot obs}/F_{CO_2\cdot fill}$). First, we used a simple linear regression to compare the half-hourly $F_{CO_2\cdot model}$ against $F_{CO_2\cdot obs}$ for each year. The comparison was also done for the daily and eight-day $F_{CO_2\cdot model}$ against $F_{CO_2\cdot fill}$ for each year. The temporal scales were selected to target the two dominant characteristic scales in the F_{CO_2} time series (i.e., daily–synoptic and seasonal–annual scales) (Baldocchi et al., 2001; Desai, 2010; Ouyang et al., 2014). The comparison of $F_{CO_2\cdot model}$ and $F_{CO_2\cdot fill}$ was made only for those periods that had less than 50% of gap-filled data. The model error statistics provided an estimate of the unexplained variation by our models, which resulted from the uncertainties both in the EC measurements and model parameterization. Second, we examined the agreement between $F_{CO_2\cdot model}$ and $F_{CO_2\cdot fill}$ at different times and timescales via wavelet coherence (Grinsted et al., 2004; Stoy et al., 2013). The "biwavelet" package was adopted to calculate the wavelet coherence across a wide range of scales (2^0–2^{13} h) (Gouhier, 2014). Following Grinsted et al. (2004), we interpreted the coherence as an estimate of correlation between two time series across times and timescales and the coherence threshold was set as 0.7 for determining the significance (i.e., >0.7 as significant coherence).

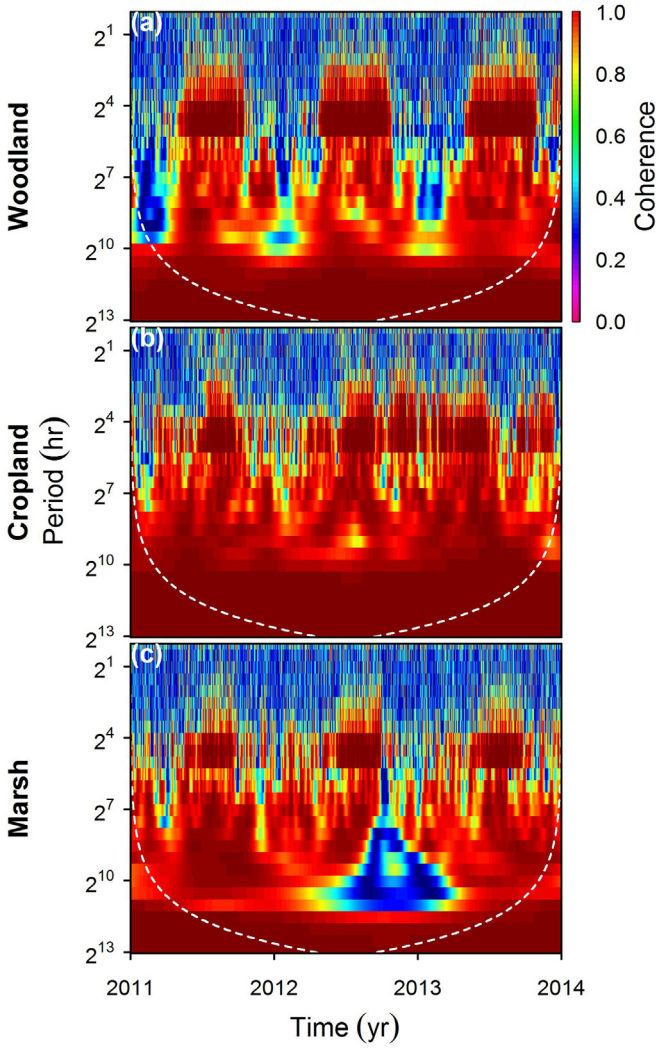

Fig. 1. Wavelet coherence between the observed (gap-filled) and modeled net ecosystem CO_2 exchanges (F_{CO_2}) along the time and timescale (period) axes. The colorbar denotes the wavelet coherence and the coherence threshold is set as 0.7 for determining the significance (i.e., >0.7 as significant coherence). The dashed lines indicate the cones of influence beyond which the wavelet coherence should not be interpreted. (For interpretation of the references to color in this figure legend, the reader is referred to the web version of the article.).

3. Results

3.1. Model diagnostics and error statistics

The modeled F_{CO_2} showed significant wavelet coherence against the observed F_{CO_2} at the half-daily to daily scale (~2^3–2^5 h) during the growing season and at the annual scale (~2^{12}–2^{13} h) through the study period at all the sites (Fig. 1). There was a longer data gap (~16 days) at the marsh site in the 2012 fall, during which the modeled F_{CO_2} deviated unmistakably from the MDS-filled F_{CO_2} (Fig. 1c). Outside this long-gap event, the simulated F_{CO_2} showed significant wavelet coherence against the observed F_{CO_2} at the multi-daily to monthly scales (~2^7–2^{10} h) at all the sites. The inter-comparison of observed/gap-filled and modeled F_{CO_2} had slopes ranging between 1.00–1.03, 0.99–1.05, and 0.97–1.08 at the half-hourly, daily, and eight-day scales (Table A5), suggesting that the model was generally robust and unbiased in duplicating the F_{CO_2} variability across the target scales at all sites.

The simulated F_{CO_2} generally replicated the interannual variability that was compatible with the gap-filled F_{CO_2} at all sites (Fig. A2). Noticeably, the simulated annual F_{CO_2} deviated from the gap-filled annual F_{CO_2} in terms of the absolute magnitudes. For the woodland and cropland sites, the net annual CO_2 uptake was consistently higher from model simulation than gap-filling (~22% and ~11%, respectively). We found the difference of cumulative F_{CO_2} occurred mostly in the non-growing seasons and was generally negligible in the growing seasons (Figs. 1 and A2). The deviations resulted mostly from a few high F_{CO_2} pulse events that were likely associated with intermittent nighttime turbulence, CO_2 outbursts after snow meltdown/ice breakup, or pulsing CO_2 release after rainfalls (at the marsh). As our current model was not designed to incorporate these intermittent events (either drivers or model structures), our model failed to reproduce these pulsing patterns and thus led to underestimation of cumulative F_{CO_2} in the non-growing seasons. However, our model simulation still succeeded in replicating the interannual variability of the annual F_{CO_2}, which was largely determined by the interannual variability of growing season F_{CO_2}. Thus, we argued that the model framework was suitable and robust for our current research purpose. The standard deviations of annual F_{CO_2} were compatible between the gap-filled and simulated data, ranging

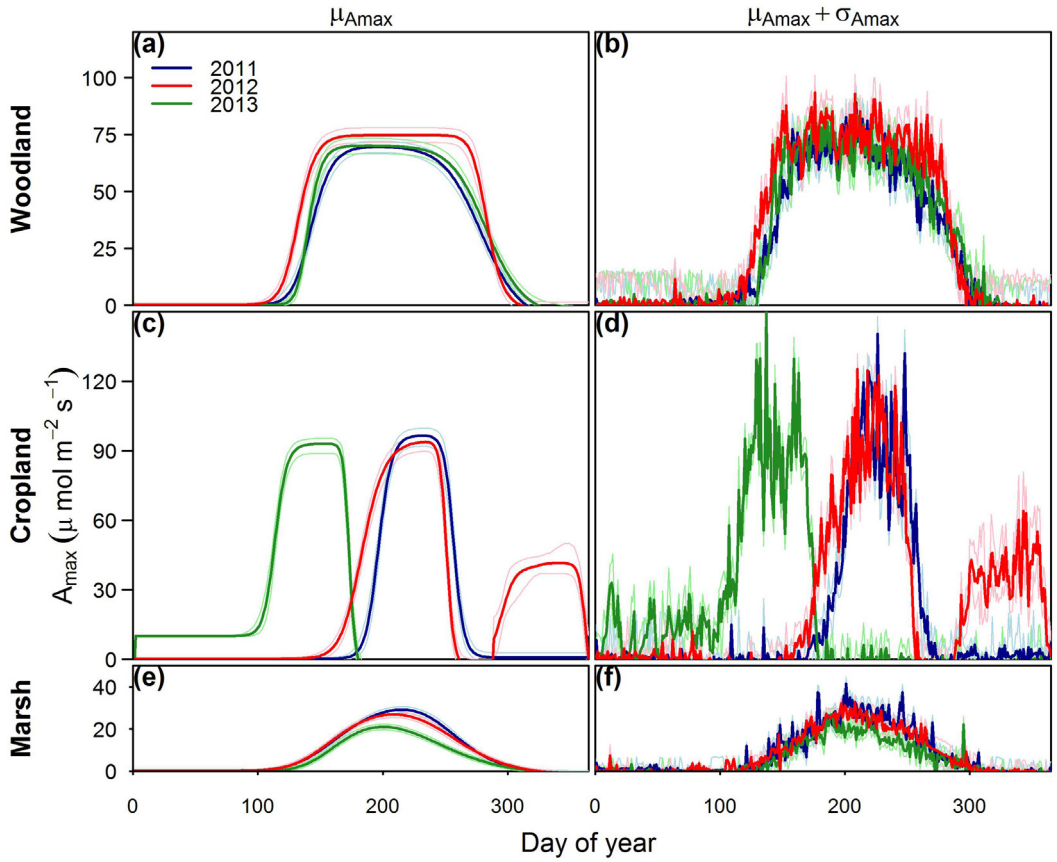

Fig. 2. Time series of the daily maximum ecosystem CO_2 uptake rate at light saturation (A_{max}), including (a, c, e) the mean estimates (μA_{max}) and (b, d, f) the means with random errors ($\mu A_{max} + \sigma A_{max}$). Light colored lines represent the 95% posterior quantile intervals. (For interpretation of the references to color in this figure legend, the reader is referred to the web version of the article.).

between 51–61, 79–84, and 86–87 g C m^{-2} yr^{-1} at the woodland, cropland, and marsh sites, respectively.

3.2. Functional parameters

Our models adequately mimicked the multi-scaled nature (multi-daily, seasonal, and interannual variability) of our target functional parameters—R_{ref} and A_{max} (Figs. 2 and 3). That allowed us to detect the interannual difference of ensemble phonological characteristics, such as the annual integrals and timing of active/peak growing periods (Fig. 2a, c, e; Fig. 3a, c, e; Fig. A3), while still preserving the information of short-term dynamics (Fig. 2b, d, f; Fig. 3b, d, f). The estimated A_{max} and R_{ref} were significantly correlated with EVI (Cor: 0.62–0.97) (Fig. A4), suggesting that their seasonal dynamics were largely associated with the ecosystem vegetation greenness.

At the woodland site, the warm year of 2012 had the longest peak assimilation periods of 125 days whereas 2011 and 2013 had 90 and 103 days, respectively, and led to the highest annual assimilation potential among the three years (Fig. 2a; Fig. A3). The earlier onset of the assimilation period in 2012 was largely associated with higher soil temperature (Fig. A4a). At the marsh site, the seasonal dynamics of A_{max} varied only marginally between 2011 and 2012 (Fig. 2e; Fig. A3a and c). The shortest duration of assimilation period (5–13 days shorter) and the lowest annual assimilation potential (29–33% lower) at the marsh were observed in 2013 (Fig. A3a and c). The cool summer of 2013 led to the lowest peak A_{max} (~20 μmol m^{-2} s^{-1}) and the senescence period started around 11–16 days earlier than in 2011 and 2012 (Fig. 2e; Fig. A3c). Noticeably, the dependence of A_{max} on soil temperature in 2013 deviated from that in 2011 and 2012 (Fig. A4i), suggesting that the early fall senescence in 2013 was influenced by other factors (e.g., chilling damage).

As expected, A_{max} at the cropland site varied greatly over the years (Fig. 2c and d) and the recovery and senescence of A_{max} did not follow closely with soil temperature (Fig. A4e). This suggested that the GEP phenology was largely influenced by agricultural management, such as crop types and plantation/harvest schedules. Considering only the periods with soybean cover, the peak A_{max}, assimilation potentials and duration of active and peak assimilation periods varied only marginally between 2011 and 2012 (Fig. 2c; Fig. A3a and c).

The ensemble characteristics of ER phenology, such as the peak R_{ref} and length of the active and peak respiration periods, also varied markedly over the years (Fig. 3e; Fig. A3b and d). The duration of peak respiration periods generally coincided with the peak assimilation periods at each site (Fig. A3c and d). This suggested that GEP and ER phenology were generally synchronized in time. As expected, the woodland site had the longest active/peak respiration periods and the highest annual respiration potential in 2012. To our surprise, the annual respiration potential was not significantly higher in 2012 at the cropland site. Also, the annual respiration potential was not significantly lower in 2013 at the marsh site. As such, the magnitudes of GEP and ER phenology (e.g., annual potentials, peak values) may not change consistently nor respond evenly to interannual climatic variability.

Yearly parameters (i.e., E_0, K_m) also varied slightly between years (Table 2). However, the difference needs to be interpreted with care. As stated earlier, these parameters tended to covary with A_{max} or R_{ref}. Therefore, treating them as separate and independent estimates may risk over-interpretation. For example,

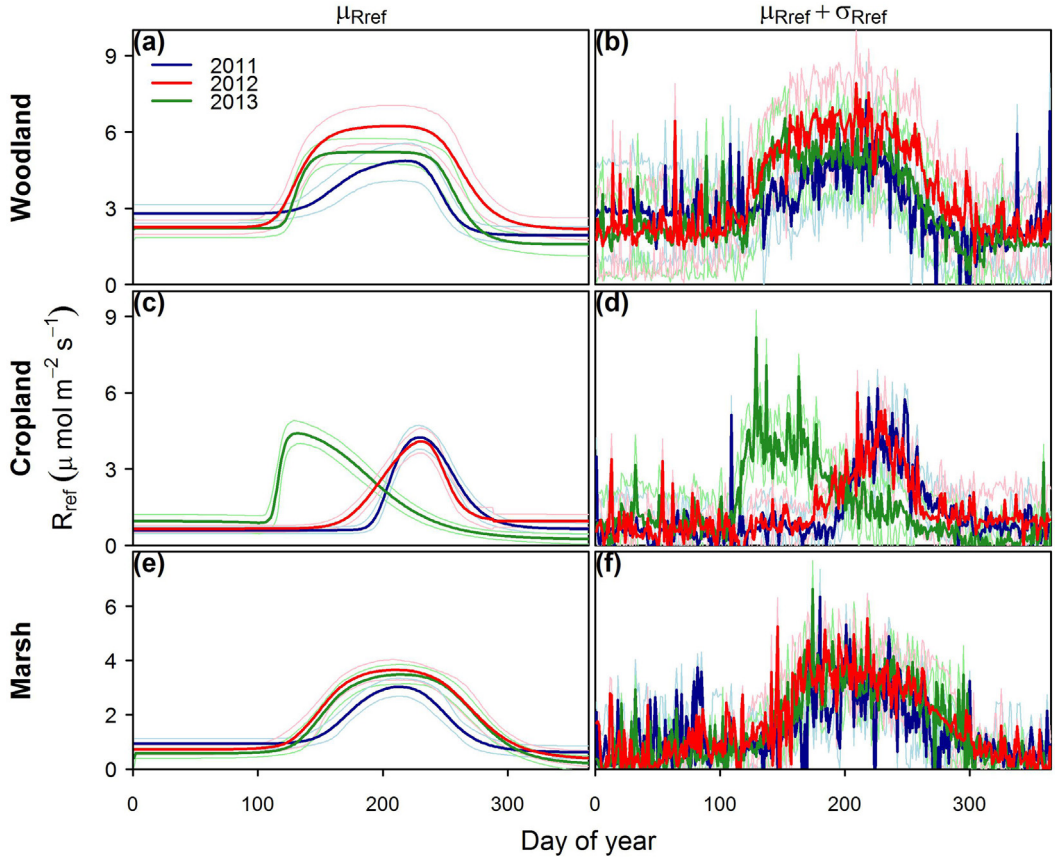

Fig. 3. Time series of the daily reference respiration (R_{ref}), including (a, c, e) the mean estimates (μ_{Rref}) and (b, d, f) the means with random errors ($\mu_{Rref} + \sigma_{Rref}$). Light-colored lines represent the 95% posterior quantile intervals. (For interpretation of the references to color in this figure legend, the reader is referred to the web version of the article.).

different E_0 was estimated among years at all the sites. This interannual difference, however, coincided with the interannual difference of peak R_{ref} (Fig. 3; Table 2). Hereafter, we treat parameters obtained from each year and each model as a set that represented the comprehensive functional status of GEP or ER for each year (e.g., 2011 parameter). The parameters from each year were used together running the cross-year model simulation and the effects of different environmental drivers in each year were not further partitioned in the study.

3.3. Direct and indirect effects on variability of local eight-day GEP, ER, and F_{CO_2}

Both direct and indirect effects explained a substantial portion of the local eight-day variation of GEP, ER, and F_{CO_2} over the years (Figs. 4–6). Additionally, their relative contribution (either in direction or in magnitude) varied substantially through time and among sites. Briefly, the local variability of GEP, ER, and F_{CO_2} at the cropland was dominantly driven by the indirect effects (Fig. 4), reflecting largely the year-to-year difference in the crop plantation and harvest schedules. The growing periods at the cropland site were relatively short, where A_{max} and R_{ref} varied drastically and rapidly. Thus, any change in the planting schedule and/or crop types produced a substantial difference in the local eight-day GEP, ER, and F_{CO_2} over the years (up to ±80, ±30, and ±60 g C m^{-2} 8d^{-1}). Woodland and marsh sites, in contrast, had relatively smaller local eight-day variability over the years that was generally bounded within ±20 and ±15 g C m^{-2} 8d^{-1} (Figs. 5 and 6).

The warm spells in spring and summer in 2011 and 2012 affected the local variability of GEP, ER, and F_{CO_2} mainly through the indirect effects that triggered the shifts of growing periods over the years (Figs. 4–6 and A1). There were direct effects on ER that were caused by warm air temperature, but the effects were marginal and generally less than ~10 g C m^{-2} 8d^{-1} at all the sites. The woodland site had ~70 and ~30 g C m^{-2} higher GEP modulated by the indirect effect in the early and late growing periods (DOY 121–153 and 257–281) in 2012 (Fig. 5a). On the other hand, the relatively drier atmosphere (higher VPD) in the late summer (DOY 217–241) in 2012 led to ~28 g C m^{-2} lower GEP through the direct effect (Fig. 5a; Fig. A1c). As ER was only slightly higher in the growing period in 2012 (~6 g C m^{-2}), the net CO_2 uptake increased ~81 g C m^{-2} at the woodland site (Fig. 5c). Similarly, the marsh site had marginally higher GEP in 2012 as a consequence of indirect effects (Fig. 6a). As GEP was less limited by the dry atmosphere at the marsh site than the woodland site, the direct effect, in contrast, enhanced the marsh GEP as a result of higher PAR in the relatively rainless summer of 2012 (Fig. 6a; Fig. A1a–c). In total, the marsh site had ~48 and ~22 g C m^{-2} higher GEP caused by the direct and indirect effects in the growing period of 2012. In contrast to the woodland site, the marsh site had higher ER in the growing period of 2012 mostly resulting from the indirect effect (~25 g C m^{-2}). Consequently, the net CO_2 uptake increased by ~29 g C m^{-2} at the marsh site in the growing period of 2012 (Fig. 6c).

The late summer cool spells of 2013 (DOY 208–239) posed a substantial and opposite effect on CO_2 fluxes at the woodland and marsh sites (Figs. 5 and 6). At the woodland site, the 32-day cumulative CO_2 uptake was ~17 g C m^{-2} higher in 2013 than the three-year average (Fig. 5c). The enhanced CO_2 uptake was largely attributed to lower ER (~38 g C m^{-2}) modulated by the indirect effects (Fig. 5b). The indirect and direct effects on GEP compensated each other to

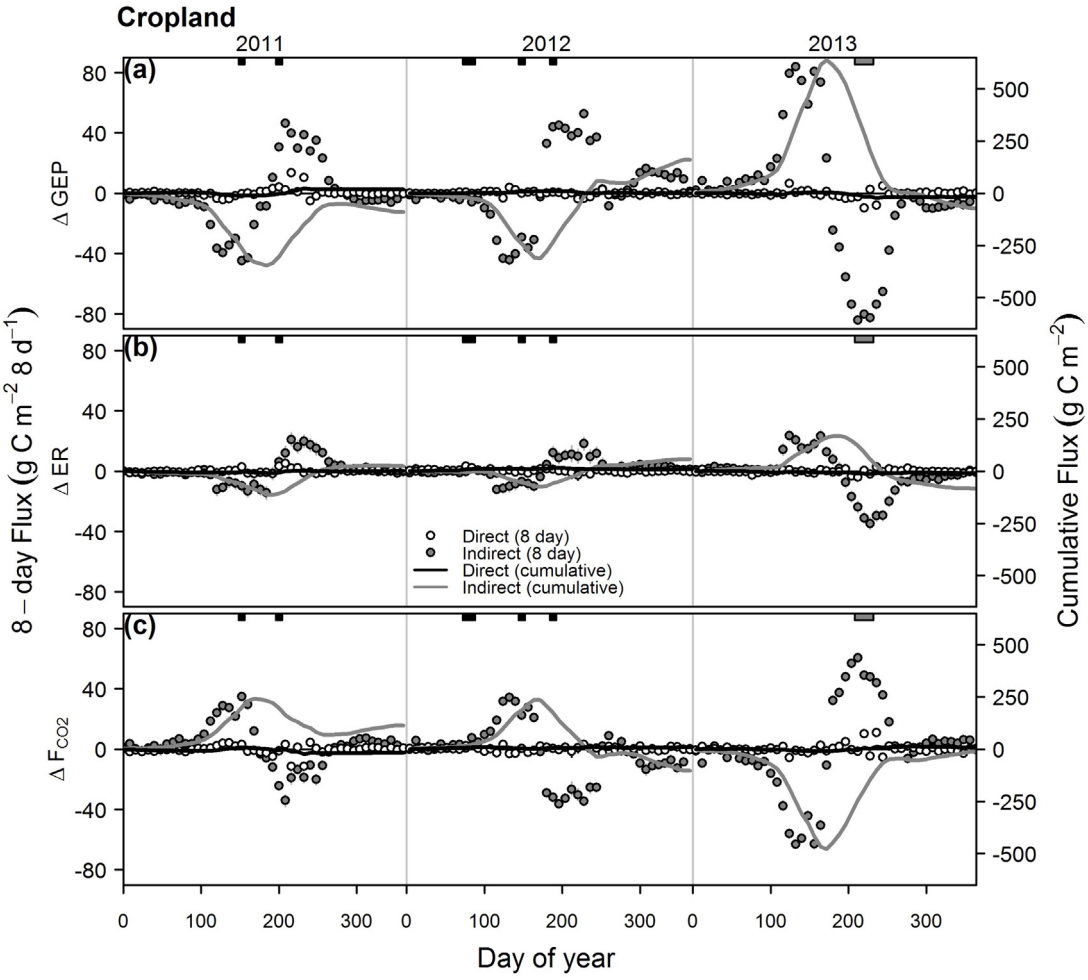

Fig. 4. The effects of year-to-year variation in environmental drivers and model parameters on modeled (a) gross ecosystem production (ΔGEP), (b) ecosystem respiration (ΔER), and (c) net ecosystem CO_2 exchange (ΔF_{CO_2}) at the cropland site. Variation of each eight-day integrated fluxes over the years was partitioned into effects of environmental drivers (direct effect) and model parameters (indirect effect). The baseline (i.e., 0) was set as the average of nine-scenario simulations in each eight-day period. The sign convention is that a positive effect on ER and GEP increases the respiration loss and assimilation uptake whereas a negative effect on F_{CO_2} increases the net ecosystem CO_2 uptake. Cumulative effects were calculated starting from the first day of each year. Vertical segments indicate the 95% quantile intervals of model simulation. Black and gray blocks indicate the duration of climate anomaly events (warm and cool spells) similar to Fig. A1a.

a large extent and led to only a ~20 g C m^{-2} decrease in GEP. The marsh site, in contrast, had a lower net CO_2 uptake during the cool summer period of 2013 of ~11 g C m^{-2} below the three-year average (Fig. 6a). Remarkably, the reduction of CO_2 uptake lasted much longer than the duration of the cool event until the end of growing period (~DOY 272). In total, the net CO_2 uptake was ~42 g C m^{-2} lower from DOY 240 to the end of growing period in 2013 in comparison with the three-year average. This lower CO_2 uptake was dominantly driven by the indirect effect on GEP (~51 g C m^{-2}, Fig. 6c) while ER was generally compatible comparing to 2011 and 2012.

3.4. Direct and indirect effects on variability of annual GEP, ER, and F_{CO_2}

Indirect effects generally explained a substantial portion of the interannual variability in annual GEP, ER, and F_{CO_2} at all the sites (Fig. 7). However, the relative contribution of direct and indirect effects varied among different CO_2 fluxes and sites. Noticeably, a large portion of the local eight-day variability at the cropland was compensated over time while integrating into annual integrals (Fig. 4 and Fig. 7c). Despite the absolute magnitudes of annual F_{CO_2} differed evidently from around −500 and −300 g C m^{-2} yr^{-1} at the woodland and cropland to near 0 g C m^{-2} yr^{-1} at the marsh, the interannual variability was surprisingly compatible and within 61–86 (SD) g C m^{-2} yr^{-1} at all the sites (Fig. 7a, c, e).

The interannual variation of annual F_{CO_2} was mainly driven by the varying parameters over the years, accounting for 54%, 89%, and 86% of the variation at the woodland, cropland, and marsh sites, respectively. Such indirect effects translated to ±85, ±110, and ±85 g C m^{-2} yr^{-1} year-to-year difference in the annual F_{CO_2} (Fig. 7b, d, f). On the other hand, the varying climate conditions over the years accounted for 33% of the interannual F_{CO_2} variation at the woodland site and became irrelevant (<10%) at the cropland and marsh sites. Such direct effects led to ±70, ±16, and ±28 g C m^{-2} yr^{-1} year-to-year difference in the annual F_{CO_2} at the woodland, cropland, and marsh sites, respectively. At all the sites, the interannual variation of GEP was dominantly driven by indirect effects, which accounted for 79–91% of interannual variation (i.e., ±96 to ± 175 g C m^{-2} yr^{-1} year-to-year difference). For ER, indirect effects dominated the interannual variation at the woodland and cropland sites (91% and 90%) while accounting for only 51% of the interannual variation at the marsh site.

The indirect effects on annual GEP and ER generally varied in the same directions over the years (Fig. 7b, d, f; Fig. A5e; Cor: 0.72).

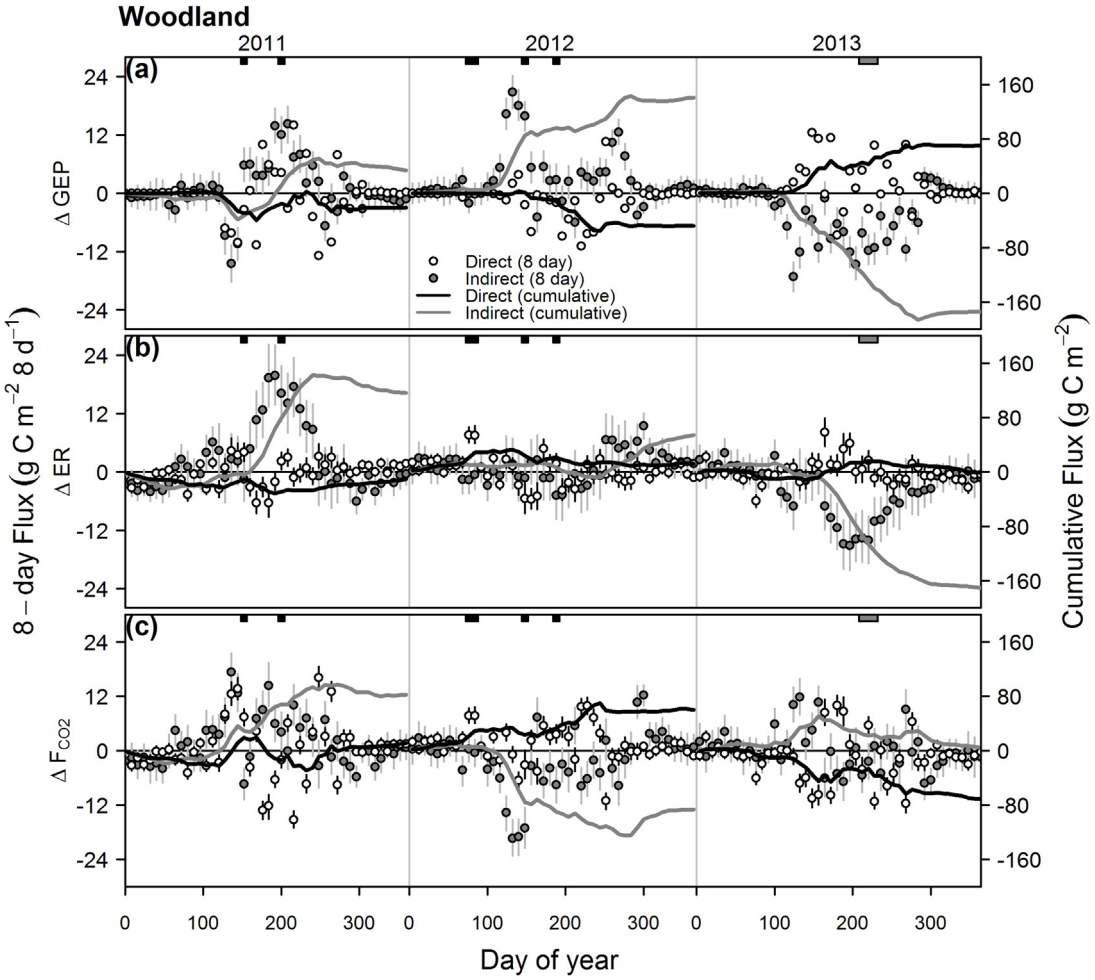

Fig. 5. The effects of year-to-year variation in environmental drivers and model parameters on modeled (a) gross ecosystem production (ΔGEP), (b) ecosystem respiration (ΔER), and (c) net ecosystem CO_2 exchange (ΔF_{CO_2}) at the woodland site. Variation of each eight-day integrated fluxes over the years was partitioned into effects of environmental drivers (direct effect) and model parameters (indirect effect). The baseline (i.e., 0) was set as the average of nine-scenario simulations in each eight-day period. The sign convention is that a positive effect on ER and GEP increases the respiration loss and assimilation uptake whereas a negative effect on F_{CO_2} increases the net ecosystem CO_2 uptake. Cumulative effects were calculated starting from the first day of each year. Vertical segments indicate the 95% quantile intervals of model simulation. Black and gray blocks indicate the duration of climate anomaly events (warm and cool spells) similar to Fig. A1a.

That means, the increase of annual GEP induced by indirect effects was usually accompanied by the increase of annual ER also induced by indirect effects. We did not find similar co-varying patterns in the direct effects on annual GEP and ER, or between the direct and indirect effects on all fluxes (Fig. A5b, c, d, f; Cor: −0.45 to 0.35). In sum, GEP and ER—the two large and opposite fluxes that determine the annual net CO_2 uptake, tend to co-vary over the years and sites. Such co-varying pattern is mostly driven by the synchronous changes (in directions) of indirect effects on GEP and ER. Consequently, the interannual variability of annual F_{CO_2} is surprisingly conservative and compatible among all the sites.

4. Discussion

4.1. Direct climatic and indirect functional effects

Our findings reiterate the important roles of functional changes in driving the interannual F_{CO_2} variability (i.e., indirect effect). Most importantly, the relative contribution of indirect effects could differ distinctly among sites, which leads to the cross-site difference of interannual F_{CO_2} variability. While several studies have attempted to address the similar research questions (Hui et al., 2003; Polley et al., 2008; Richardson et al., 2007; Shao et al., 2014; Teklemariam et al., 2010; Wu et al., 2012), very few of them were conducted using such a cluster-wise experiment design. Thus, previous studies often constrained their scopes on either the long-term variability in one single site (e.g., Richardson et al., 2007; Wu et al., 2012) or a generalized overview of multiple sites from diverse climate zones and geo-locations (e.g., Shao et al., 2014, 2015). Often, those multi-site studies had to ignore the details of site-specific climatic conditions and the comparisons were carried out on simple metrics derived at the annual to interannual scales. The discrepancy in model structures further limited the capability in interpreting the varied results among studies.

In our case, we were able to partition the interannual variation at both the local and annual scales and examine the partitioned effects through times and across sites. Our study clearly showed that different ecosystems responded differently to such similar climatic forcing. The interannual F_{CO_2} variability was larger (79 and 86 g C m^{-2} yr^{-1}) and dominated by indirect effects (89% and 86%) at the cropland and marsh sites. On the other hand, the interannual F_{CO_2} variability and indirect effect were marginally lower at the woodland site (61 g C m^{-2} yr^{-1} and 54%). Our findings concurred with the proposition in Shao et al. (2015) that the cross-site difference of interannual F_{CO_2} variability was largely determined by the difference of indirect effects among sites.

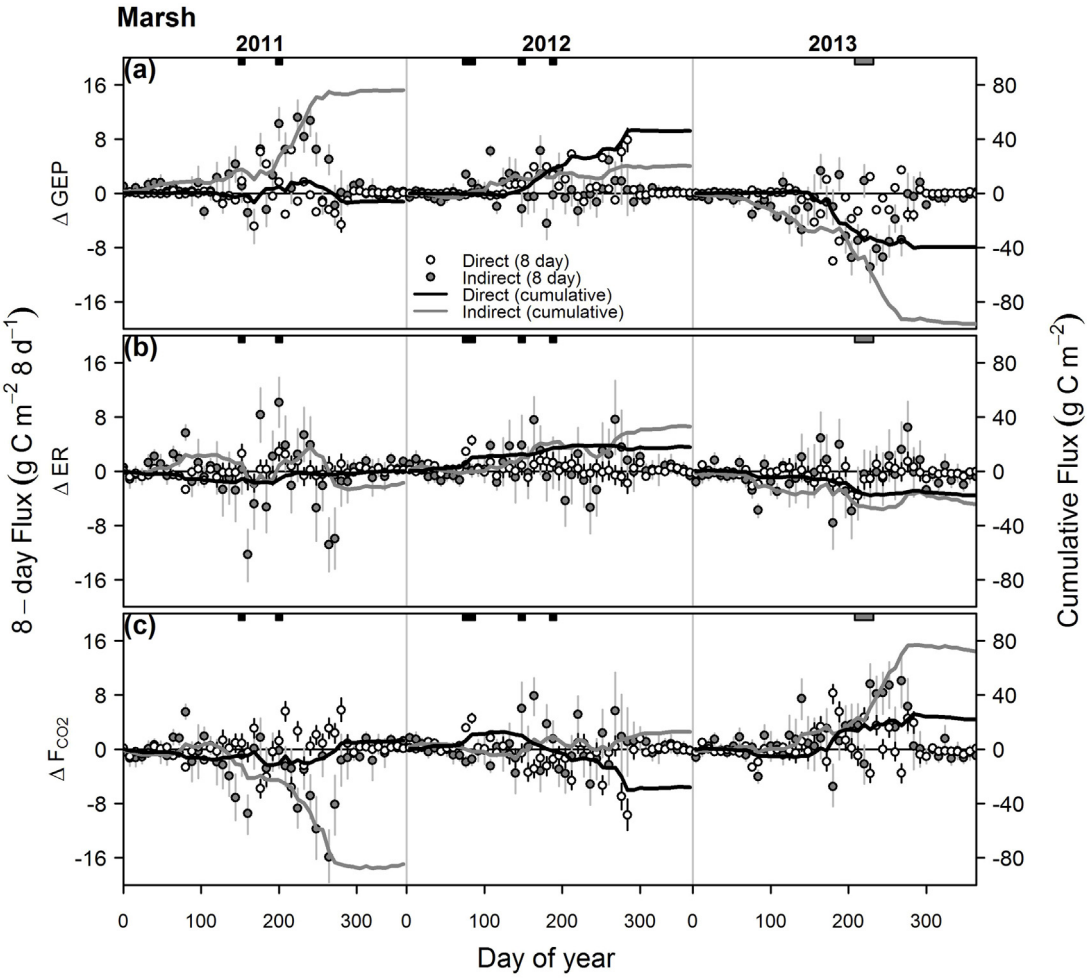

Fig. 6. The effects of year-to-year variation in environmental drivers and model parameters on modeled (a) gross ecosystem production (ΔGEP), (b) ecosystem respiration (ΔER), and (c) net ecosystem CO_2 exchange (ΔF_{CO_2}) at the marsh site. Variation of each eight-day integrated fluxes over the years was partitioned into effects of environmental drivers (direct effect) and model parameters (indirect effect). The baseline (i.e., 0) was set as the average of nine-scenario simulations in each eight-day period. The sign convention is that a positive effect on ER and GEP increases the respiration loss and assimilation uptake whereas a negative effect on F_{CO_2} increases the net ecosystem CO_2 uptake. Cumulative effects were calculated starting from the first day of each year. Vertical segments indicate the 95% quantile intervals of model simulation. Black and gray blocks indicate the duration of climate anomaly events (warm and cool spells) similar to Fig. A1a.

To date, there is no consensus of what leads to the difference of the contribution of indirect effects across sites. We argue that the histories and regimes (e.g., intensity, frequency) of natural and human disturbance may explain at least a portion of the cross-site difference. Polley et al. (2008) examined the interannual F_{CO_2} variability at two nearby prairie sites with different grazing management (grazed vs. ungrazed). They found that grazing management reduced the influence of plants on ecosystem carbon processes. For example, it reduced the F_{CO_2} variability generated by plant physiological and phenological changes and it altered the most relevant environmental drivers in explaining the F_{CO_2} variability. A similar conclusion was made in McVeigh et al. (2014) and Teklemariam et al. (2010), where ecosystems mediated the response of CO_2 fluxes to climatic variability through a different degree of structural and functional modification in the dominant vegetation. Teklemariam et al. (2010) argued that the difference among ecosystems may be attributed to their different histories of natural and human disturbance. The interannual F_{CO_2} variability tends to be mainly driven by external environmental variability in ecosystems that adjust to prolonged exposure of a given environmental condition, such as the 70-year-old woodland in our study. In contrast, ecosystems that are prone to frequent disturbance and management, such as the cropland in our case, tend to have the interannual F_{CO_2} variability mainly driven by indirect effects.

Further research should focus on generating a suitable framework to better quantify the effects of the disturbance history and regime. Shao et al. (2015) argued that higher disturbance intensity may not always lead to higher contribution of indirect effects. Different disturbance regimes may also influence the interplay of direct and indirect effects. Currently, the data are still insufficient to draw a general conclusion about the influence of disturbance regimes. Further studies with a more sophisticated design (e.g., paired or cluster-wise sites) are required in order to disentangle the explicit roles of disturbance regimes.

While the importance of indirect (or biotic/parameter) effects on interannual F_{CO_2} variability has been discussed in several studies (Hui et al., 2003; Polley et al., 2008; Richardson et al., 2007; Shao et al., 2014; Teklemariam et al., 2010; Wu et al., 2012), challenges remain in synthesizing these reports and interpreting the indirect effects. Extra caution is required because different statistical models are adopted in partitioning the direct/indirect effects. Those models are fundamentally different in their structure and/or statistical assumptions. Thus, the different partitioned variation among reports reflects to an unknown extent the inherent model differences (Shao et al., 2015; Wu et al., 2012). Potentially, the indirect

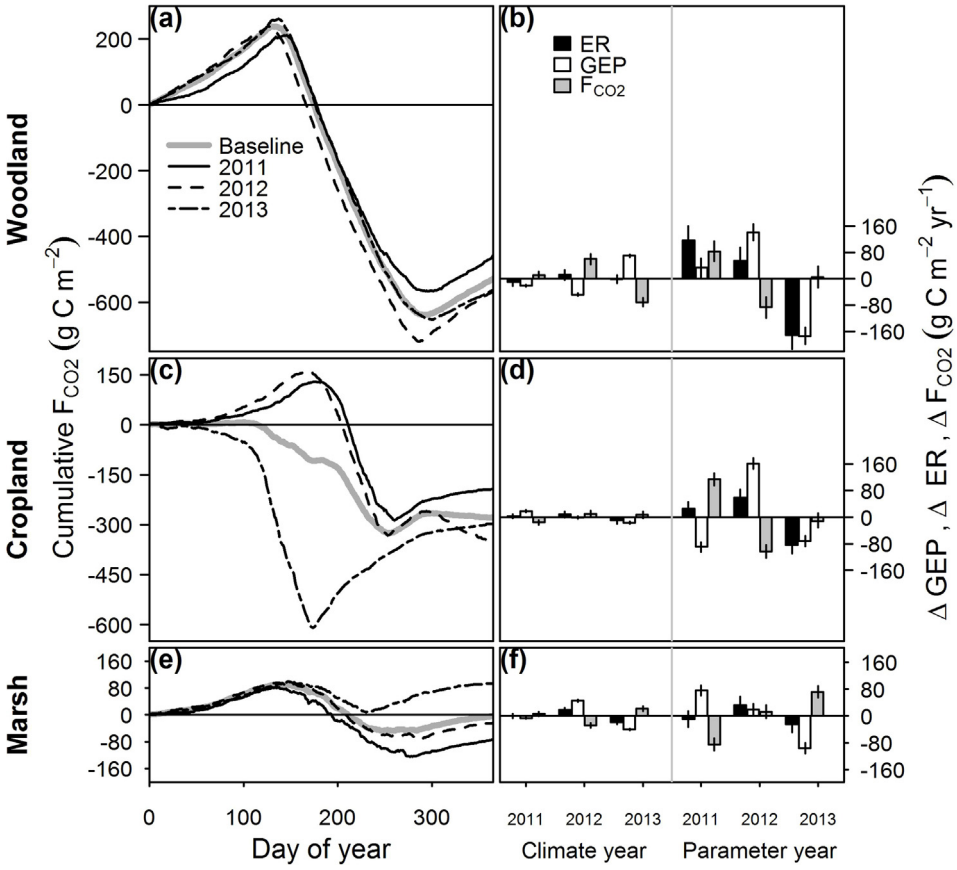

Fig. 7. Annual cumulative net ecosystem CO_2 exchange (F_{CO_2}) (a, c, e) and the effects of environmental drivers (climate year) and model parameters (parameter year) (b, d, f) on annual F_{CO_2} (ΔF_{CO_2}), gross ecosystem production (ΔGEP), and ecosystem respiration (ΔER). The baseline F_{CO_2} was obtained from the average of nine-scenario simulations at each site (Fig. 7a, c, e) and then used as the reference level (i.e., 0) in presenting the direct and indirect effects in Fig. 7b, d, f. The sign convention in Fig. 7b, d, f is that a positive effect on ER and GEP increases the respiration loss and assimilation uptake whereas a negative effect on F_{CO_2} increases the net ecosystem CO_2 uptake. The effects that are caused by the interactions between the climate and parameter years are generally minor and are not presented here. Vertical segments in Fig. 7b, d, f showed the 95% quantile intervals of model simulation.

effects involve the changes of structural, physiological, and phenological traits of ecosystems (Humphreys and Lafleur, 2011; Luo et al., 2001; Richardson et al., 2010). Different models may or may not be capable of replicating the variation as induced by all those changes.

Additionally, unaccounted environmental drivers or prolonged and lagged effects that were not incorporated in the model structure may also contribute to the indirect effects (Ciais et al., 2005; Desai, 2014). Contrary to other studies (Baldocchi et al., 2005; Richardson et al., 2007), we did not use soil temperature as a predictor variable in modeling the spring recovery and fall senescence of GEP and ER. By incorporating soil temperature, a portion of the current indirect effects at the woodland and marsh sites could be partitioned into the direct effects of soil temperature (Fig. A4). Interestingly, the strong relationship between the EVI and A_{max}/R_{ref} suggested a potential avenue for further model improvement. Currently, challenges remain in adequately incorporating these snap-shot/satellite-based vegetation indices (e.g., every 8–16 days) into our model framework. We suggest future studies should incorporate near-surface continuous phenological measurements (e.g., radiometric sensors, digital cameras) (Ryu et al., 2012; Soudani et al., 2012; Toomey et al., 2015). Thus, the changes in plant phenology can be directly incorporated as predictor variables and the phenological effects can be distinguished from the current indirect effects.

4.2. Influence of climatic variability and anomaly

Recent climatic variability and anomalies in the Great Lakes region provided us a rare and valuable opportunity to examine the interannual F_{CO_2} variability across different ecosystems. With these record-breaking climate anomalies, we were able to examine how ecosystem carbon processes may respond to the extreme and contrasting climatic conditions (e.g., wet-dry, warm-cool) in a relative short time span (~3 years). Most importantly, the similar climatic variability across the region allowed us to closely and simultaneously examine the response of F_{CO_2} variability in different ecosystems. In general, the year-to-year changes of GEP and ER correlated positively with each other when pooling all the site-year data (i.e., high annual GEP with high annual ER) (Cor: 0.73; Fig. A5a). The positive correlation is of great importance because it implies that year-to-year variation of GEP and ER partly compensate each other, which dampens the interannual variability of F_{CO_2} (Baldocchi, 2008). The year-to-year changes of GEP and ER did not synchronize across sites (to be discussed below), suggesting that different ecosystems responded differently to similar climate conditions in a specific year. We did not find evident correlations between the direct and indirect effects as reported in Shao et al. (2014) (Fig. A5b, d, f). This lack of correlation suggests that ecosystem functional changes may not always compensate or supplement the direct/instantaneous effects driven by environmental

forcing (neither synergistically nor antagonistically) (Richardson et al., 2007; Shao et al., 2014).

Both the woodland and cropland sites had the highest net CO_2 uptake in the warm year of 2012 mainly because of longer peak assimilation periods and higher assimilation potentials. The marsh, in contrast, had lower net CO_2 uptake in 2012 than in 2011 because the increase of ER exceeded the increase of GEP. Contrasting effects of an earlier warm spring on net annual CO_2 uptakes were reported in several studies across a diverse range of ecosystems in boreal and temperate regions (e.g., Hu et al., 2010; Kross et al., 2014; Lafleur and Humphreys, 2008; Richardson et al., 2009, 2010). At the woodland site, the warm temperature in 2012 had the most influence through triggering earlier onsets of active/peak assimilation periods and leading to higher annual assimilation potentials. Similar findings were reported in previous studies showing that warm springs tend to enhance GEP more than ER in forest ecosystems (Black et al., 2000; Richardson et al., 2010).

On the other hand, the net CO_2 uptake in wetlands may not always benefit from a warmer climate condition (Sulman et al., 2010). As wetlands often accumulate a substantial amount of carbon from allochthonous and autochthonous sources, the increase of ER may exceed the increase of GEP during the warm years when more labile carbon becomes available for decomposition as a consequence of a relatively lower water table (Chu et al., 2015; Lafleur et al., 2003). Similarly, the effects of the warm spring on CO_2 uptake in croplands are less clear because the planting schedule is often determined based on more than just one single factor (i.e., soil temperature). In our case, both the warm temperature and relatively low precipitation during April–May (and thus adequate soil water status) in the 2012 spring provided favorable conditions for early cultivation. Thus, soybeans were planted ~20 days earlier in 2012 than that in 2011, when frequent precipitation led to near-saturated soil water content postponing the cultivation schedule.

The cool spells in the 2013 summer influenced the marsh CO_2 uptake via reducing the assimilation potential and GEP. The woodland site, in contrast, had slightly higher annual CO_2 uptake than the three-year average as a consequence of reduced ER. We found that the cool events triggered early senescence and caused the peak assimilation period to end much earlier in 2013 at the marsh than in 2011 or 2012. The mechanisms of the cool-spell effects remain unclear and have not been reported in previous wetland studies. In general, lower temperature led to earlier senescence, which explained a large portion of the observed lower GEP. However, we found that the response curves of A_{max} and R_{ref} against soil temperature in 2013 deviated from those in 2011 or 2012, suggesting that other factors (e.g., chilling damage) may also play an important role.

5. Conclusions

With only three years of data, we are cautious about drawing a generalized conclusion about the interannual variability and long-term baseline of CO_2 fluxes at the three ecosystems. However, the simultaneous CO_2 flux observation at multiple ecosystems that experienced similar climate variability and anomaly certainly provide valuable insights in how contrasting ecosystems may respond to similar environmental forcing. The positive correlation between the year-to-year changes of GEP and ER suggests that GEP and ER generally compensate each other to a large extent, leading to a decrease in the climate sensitivity of interannual F_{CO_2}. Such co-varying GEP-ER pattern is largely driven by nearly synchronous changes in the indirect effects of GEP and ER. Thus, even when climate conditions vary drastically in our three-year study period, the variability of the annual F_{CO_2} (SD: 61–86 g C m^{-2} yr^{-1}) is still conservative and within the reported ranges from cross-site/cross-year synthesis.

Our findings also highlight that changes in functional parameters (e.g., A_{max}, R_{ref}) over the years play an important role in driving the interannual F_{CO_2} variability (54–89%) at all the sites. The year-to-year changes of GEP/ER did not synchronize across sites. Consequently, different ecosystems may respond differently to similar climatic conditions in a specific year in terms of annual net CO_2 uptakes. While the warm temperature in the spring of 2012 triggered the growing season in the woodland site to start earlier and substantially increased the annual CO_2 uptakes, similar conditions turned the marsh to near CO_2 neutral because of enhanced ER. Similarly, the cool spell in the summer of 2013 also influenced GEP and ER differently in different ecosystems that responded oppositely in their annual CO_2 uptake. Future research should focus on the unequal response among ecosystems to similar climatic variability in order to better predict, upscale, and assess the potential impacts of future climate change.

Acknowledgements

This project was funded by the National Oceanic and Atmospheric Administration (NOAA) (NA10OAR4170224), USA. We thank John Simpson and the Winous Point Marsh Conservancy for supporting the research platform at the Winous Point North Marsh and Walter Berger for providing his cropland and helping with the infrastructure construction. Tim Schetter, Karen Menard, Russ Maneval, and the Metroparks of the Toledo Area allowed us access to the Oak Openings Preserve Park and offered logistical support. Ge Sun and Richard Becker gave helpful advice. We gratefully acknowledge Mike Deal, Jianye Xu, Changliang Shao, Yahn-Jauh Su, Jing Xie, Jennifer Teeple, Terenzio Zenone, Michael Abraha, Wei Shen, Angela Fan, Xiaosong Zhang, and Susie Wu for building and maintaining the site infrastructure and assisting with data management. We also thank Gabriela Shirkey for editing the manuscript.

Appendix A. Implications of the modeling approach

Our attempts to utilize a structurally simple and flexible Bayesian hierarchical model provide insights into future ER-GEP modeling. First, the observed time series of F_{CO_2} is often composed

Table A1
Summary of the phenological indices.

Phenological Indices	Interpretation
Annual assimilation potential (AAP)	The maximal annual assimilation rate that is not limited by PAR and VPD
Annual respiration potential (ARP)	The annual respiration potential under the reference temperature (10 °C)
Peak assimilation capacity/reference respiration	The peak assimilation rate/reference respiration
Assimilation/respiration up-turn day (t_U)	The theoretical starting day for active assimilation/respiration period
Assimilation/respiration stabilization day (t_S)	The theoretical starting day for peak assimilation/respiration period
Assimilation/respiration down-turn day (t_D)	The theoretical ending day for peak assimilation/respiration period
Assimilation/respiration recession day (t_R)	The theoretical ending day for active assimilation/respiration period
Length of active assimilation/respiration period	Duration of the active assimilation/respiration period
Length of peak assimilation/respiration period	Duration of the peak assimilation/respiration period

See Gu et al. (2009) for more details of the phenological indices.

Table A2
Medians and 95% quantile intervals (2.5%, 97.5%) of the posterior distributions and the lower and upper bounds [lower, upper] of the uniform prior distributions of model parameters at the woodland site. Parameter definition can be found in the main text (Eq. (10)).

Parameter	Posterior			Prior
	2011	2012	2013	Hyper parameter
$y_{0.ER}$	2.8 (2.4, 3.1)	2.3 (2.0, 2.5)	2.2 (1.9, 2.5)	[0,5]
$a_{1.ER}$	2.2 (1.3, 3.4)	4.0 (3.3, 4.9)	3.0 (2.5, 3.6)	[0,8]
$a_{2.ER}$	3.1 (2.2, 4.1)	4.1 (3.3, 5.0)	3.6 (3.1, 4.3)	[0,8]
$b_{1.ER}$	19.0 (8.5, 31.3)	12.6 (6.6, 20.2)	6.3 (5.0, 10.3)	[1,40]
$b_{2.ER}$	10.3 (5.7, 16.1)	16.1 (8.2, 25.0)	12.3 (6.9, 20.3)	[1,40]
$c_{1.ER}$	6.0 (1.8, 9.7)	5.3 (1.3, 9.7)	5.8 (1.5, 9.7)	[1,10]
$c_{2.ER}$	5.3 (1.2, 9.6)	5.7 (1.5, 9.7)	5.8 (1.6, 9.7)	[1,10]
$t_{1.ER}$	124 (98, 158)	109 (91, 130)	117 (106, 129)	[80,170]
$t_{2.ER}$	229 (209, 248)	234 (211, 259)	234 (212, 261)	[190,280]
$y_{0.GEP}$	0.2 (0.0, 0.8)	0.2 (0.0, 0.8)	0.2 (0.0, 0.8)	[0,1]
$a_{1.GEP}$	70.0 (67.3, 72.5)	74.5 (71.2, 77.8)	70.0 (66.4, 73.3)	[0,80]
$a_{2.GEP}$	78.0 (73.7, 79.9)	76.5 (72.1, 79.7)	75.5 (70.3, 79.6)	[0,80]
$b_{1.GEP}$	9.1 (7.0, 11.5)	7.4 (6.1, 9.4)	5.8 (5.1, 7.3)	[1,35]
$b_{2.GEP}$	16.2 (13.6, 19.1)	7.4 (5.8, 9.2)	16.0 (13.1, 19.5)	[1,35]
$c_{1.GEP}$	1.6 (1.0, 3.2)	1.3 (1.0, 2.9)	2.0 (1.2, 4.5)	[1,10]
$c_{2.GEP}$	1.1 (1.0, 1.6)	1.7 (1.3, 3.4)	1.3 (1.0, 1.9)	[1,10]
$t_{1.GEP}$	138 (128, 143)	129 (121, 133)	135 (128, 139)	[80,170]
$t_{2.GEP}$	277 (268, 280)	279 (272, 279)	278 (269, 279)	[190,280]

of processes at multiple temporal scales (e.g., hourly, diurnal, synoptic, seasonal, interannual) (Baldocchi et al., 2001; Ouyang et al., 2014; Stoy et al., 2005). The superimposed characteristics pose challenges in constructing a suitable model that can duplicate and predict the carbon fluxes across a wide range of temporal scales (Desai, 2014). Often, the time series has to be divided and grouped according to the target scales (e.g., by year, by season) and fitted with separate sets of model parameters. In this case, the groups are

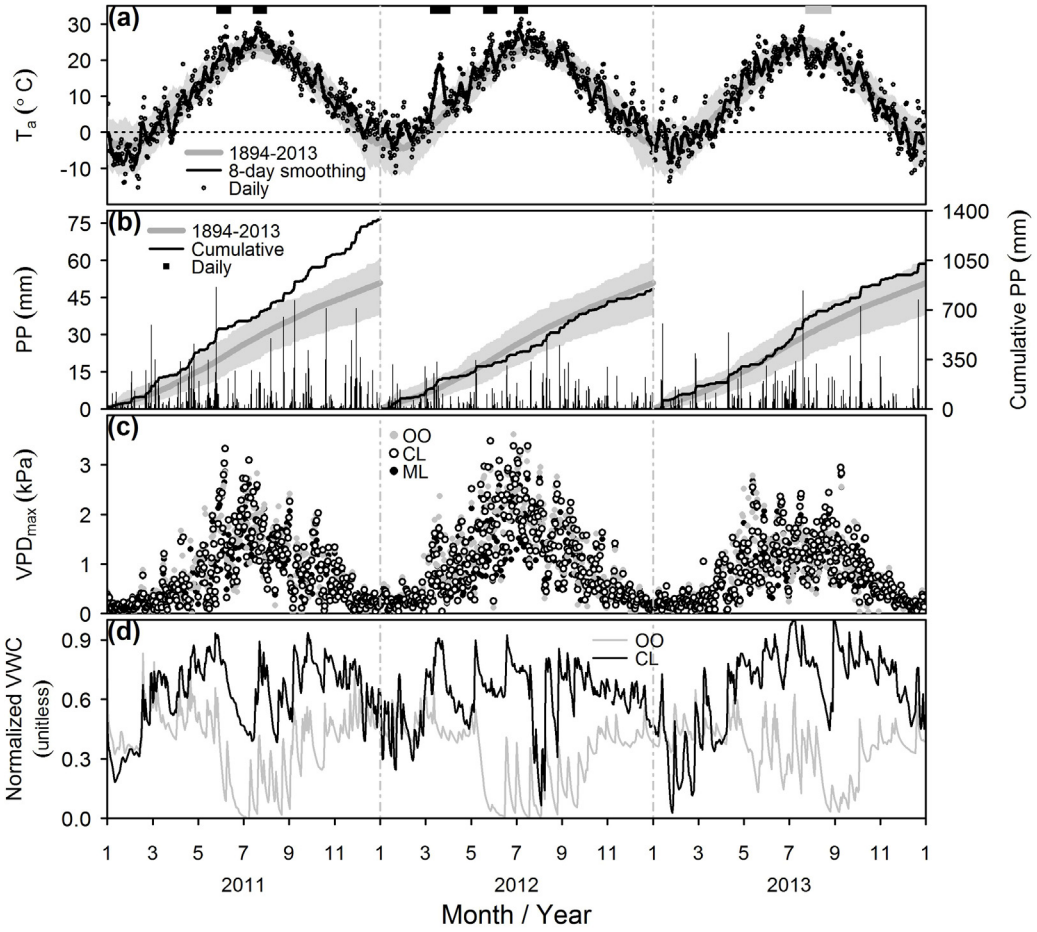

Fig. A1. Time series of the daily (a) air temperature (T_a, black circles), (b) precipitation (PP, black bars), (c) maximum vapor pressure deficit (VPD_{max}), and (d) normalized volumetric soil water content (VWC). T_a and PP were obtained from three long-term weather stations in the region. Long-term (1894–2013) average (gray lines) and its 90% quantile intervals (gray shaded areas) are presented in Fig. A1a and b. Eight-day smoothing T_a (black lines) and cumulative PP (black lines) are also showed in Fig. A1a and b. VWC is normalized by the observed ranges at each site with a full range of 0–1. Black and gray blocks in Fig. A1a indicate the durations of target climate anomaly events (warm and cool spells).

Table A3
Medians and 95% quantile intervals (2.5%, 97.5%) of the posterior distributions and the lower and upper bounds [lower, upper] of the uniform prior distributions of model parameters at the marsh site. Parameter definition can be found in the main text (Eq. (10)).

Parameter	Posterior			Prior
	2011	2012	2013	Hyper parameter
$y_{0.ER}$	0.9 (0.7, 1.1)	0.7 (0.5, 0.9)	0.6 (0.4, 0.8)	[0,5]
$a_{1.ER}$	2.7 (1.8, 3.7)	3.0 (2.5, 3.8)	3.0 (2.5, 3.7)	[0,4]
$a_{2.ER}$	3.0 (2.1, 3.9)	3.4 (2.9, 3.9)	3.4 (2.8, 3.9)	[0,4]
$b_{1.ER}$	19.6 (7.4, 32.7)	15.8 (7.1, 27.2)	15.6 (8.1, 27.3)	[1,40]
$b_{2.ER}$	16.7 (6.4, 26.7)	21.6 (12.8, 32.1)	20.7 (13.3, 31.7)	[1,40]
$c_{1.ER}$	3.6 (1.3, 9.4)	2.3 (1.0, 9.0)	2.6 (1.1, 8.9)	[1,10]
$c_{2.ER}$	2.1 (1.0, 8.8)	2.7 (1.1, 8.9)	3.0 (1.1, 9.1)	[1,10]
$t_{1.ER}$	148 (108, 169)	134 (95, 153)	134 (96, 153)	[80,170]
$t_{2.ER}$	235 (193, 256)	247 (200, 276)	248 (202, 274)	[190,280]
$y_{0.GEP}$	0.1 (0.0, 0.4)	0.1 (0.0, 0.3)	0.1 (0.0, 0.2)	[0,1]
$a_{1.GEP}$	34.2 (29.8, 38.0)	33.1 (27.8, 37.2)	33.2 (22.3, 37.8)	[0,40]
$a_{2.GEP}$	36.0 (30.2, 39.7)	35.4 (29.5, 39.8)	34.9 (23.9, 39.7)	[0,40]
$b_{1.GEP}$	24.4 (17.6, 29.3)	23.2 (15.2, 29.2)	22.0 (13.4, 28.5)	[1,35]
$b_{2.GEP}$	21.8 (15.0, 21.1)	25.7 (18.3, 32.0)	29.4 (22.2, 34.4)	[1,35]
$c_{1.GEP}$	3.2 (1.1, 6.0)	3.1 (1.2, 6.3)	3.7 (1.3, 6.8)	[1,10]
$c_{2.GEP}$	2.6 (1.1, 6.3)	1.9 (1.0, 5.8)	1.2 (1.0, 3.2)	[1,10]
$t_{1.GEP}$	132 (111, 160)	132 (109, 159)	132 (113, 157)	[80,170]
$t_{2.GEP}$	234 (203, 259)	237 (195, 261)	231 (194, 249)	[190,280]

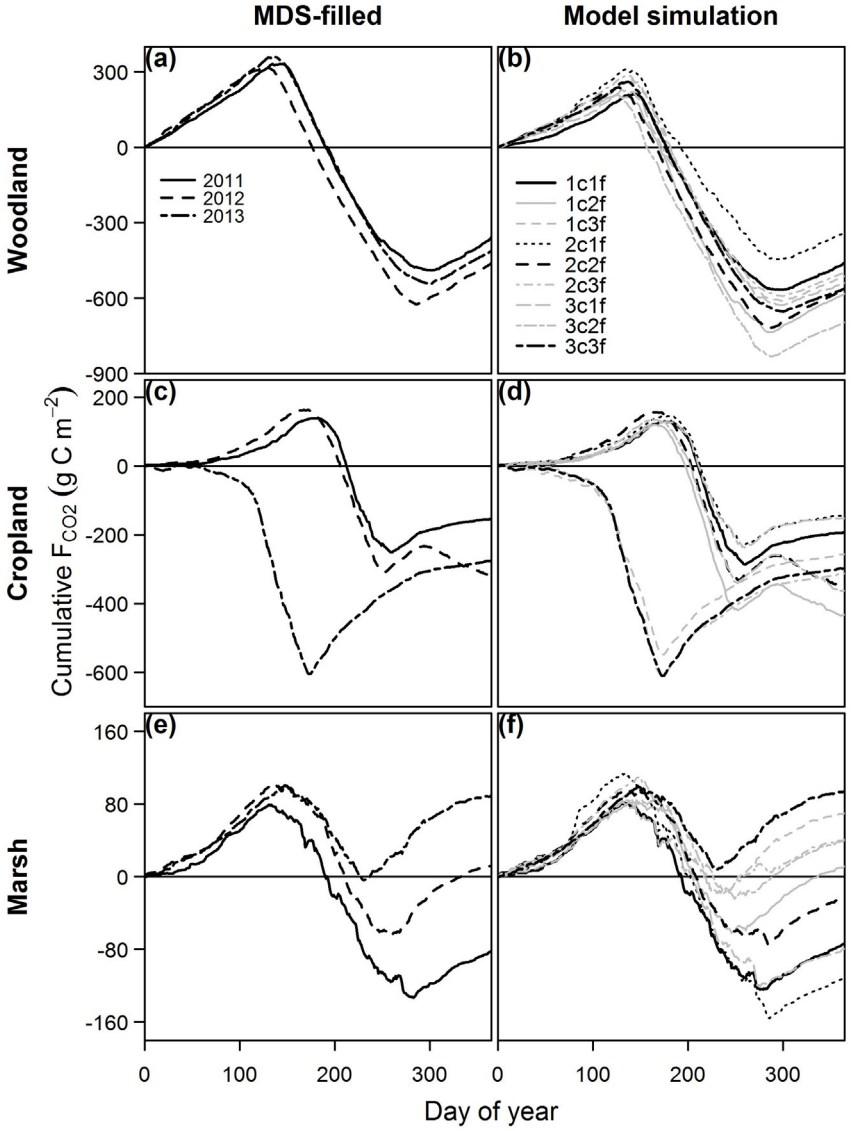

Fig. A2. Annual cumulative net ecosystem CO_2 exchange (F_{CO_2}), including (a, c, e) the gap-filled F_{CO_2} using the marginal distribution sampling method (MDS-filled) and cross-year simulated F_{CO_2} (b, d, f). Cumulative F_{CO_2} was modeled by crossing the environmental driver years with model parameter years (e.g., 2011 climate × 2011 parameter, labeled as 1c1f) in Fig. A2b, d, f.

Table A4
Medians and 95% quantile intervals (2.5%, 97.5%) of the posterior distributions and the lower and upper bounds [lower, upper] of the uniform prior distributions of model parameters at the cropland site. Parameter definition can be found in the main text (Eq. (10)).

Parameter	Posterior			Prior
	2011	2012	2013[b]	Hyper parameter
$y_{0.ER}$	0.6 (0.5, 0.7)	0.7 (0.5, 0.8)	1.0 (0.7, 1.2)	[0,5]
$a_{1.ER}$	4.2 (3.4, 5.6)	4.4 (3.5, 5.8)	3.8 (3.1, 4.9)	[0,8]
$a_{2.ER}$	4.1 (3.3, 5.6)	4.1 (3.1, 5.4)	4.5 (3.8, 5.7)	[0,8]
$b_{1.ER}$	8.9 (5.4, 14.4)	20.0 (14.0, 28.7)	3.6 (1.4, 6.4)	[1,40]
$b_{2.ER}$	14.6 (8.7, 21.0)	9.5 (4.9, 15.9)	31.6 (23.4, 39.0)	[1,40]
$c_{1.ER}$	3.4 (1.3, 8.3)	2.8 (1.2, 6.9)	3.5 (1.4, 8.4)	[1,10]
$c_{2.ER}$	3.1 (1.2, 7.9)	3.3 (1.3, 8.1)	2.4 (1.2, 6.4)	[1,10]
$t_{1.ER}$	193 (179, 205)	177 (151, 201)	110 (102, 116)	[120,210][a] [−70,120][b]
$t_{2.ER}$	238 (214, 254)	237 (220, 248)	160 (130, 179)	[190,280][a] [120,200][b]
$y_{0.GEP}$	0.2 (0.0, 0.8)	0.2 (0.0, 0.7)	0.2 (0.0, 0.8)[c] 9.8 (9.7, 10.0)[d]	[0,1][ad] [0,10][c]
$a_{1.GEP}$	96.5 (91.9, 99.8)	94.1 (89.9, 97.6)	41.4 (36.7, 63.1)[c] 83.0 (78.9, 85.4)[d]	[0,100]
$a_{2.GEP}$	96.1 (90.9, 99.6)	98.0 (93.1, 99.8)	72.8 (40.8, 97.9)[c] 98.2 (93.8, 99.8)[d]	[0,100]
$b_{1.GEP}$	4.5 (4.4, 6.7)	9.6 (7.8, 11.9)	5.8 (2.2, 25.2)[c] 4.8 (3.6, 6.3)[d]	[1,35]
$b_{2.GEP}$	4.3 (3.2, 5.6)	3.0 (2.2, 4.0)	3.5 (1.4, 7.0)[c] 2.6 (1.9, 3.5)[d]	[1,35]
$c_{1.GEP}$	1.1 (1.0, 1.9)	1.3 (1.0, 3.0)	1.2 (1.0, 2.7)[c] 1.1 (1.0, 2.0)[d]	[1,10]
$c_{2.GEP}$	1.2 (1.0, 4.0)	1.3 (1.0, 3.6)	1.4 (1.0, 4.7)[c] 1.3 (1.0, 3.6)[d]	[1,10]
$t_{1.GEP}$	196 (191, 197)	180 (168, 185)	−72 (−77, −57)[c] 112 (107, 114)[d]	[120,210][a] [−78,−36][c] [60,150][d]
$t_{2.GEP}$	256 (249, 258)	250 (246, 252)	−5 (−11, −1)[c] 171 (167, 173)[d]	[190,280][a] [−36,0][c] [120,200][d]

[a] For soybean periods (2011 to September 2012).
[b] For wheat period (September 2012–2013).
[c] For winter wheat periods (September 2012 to December 2012).
[d] For spring wheat periods (January 2013 to December 2013).

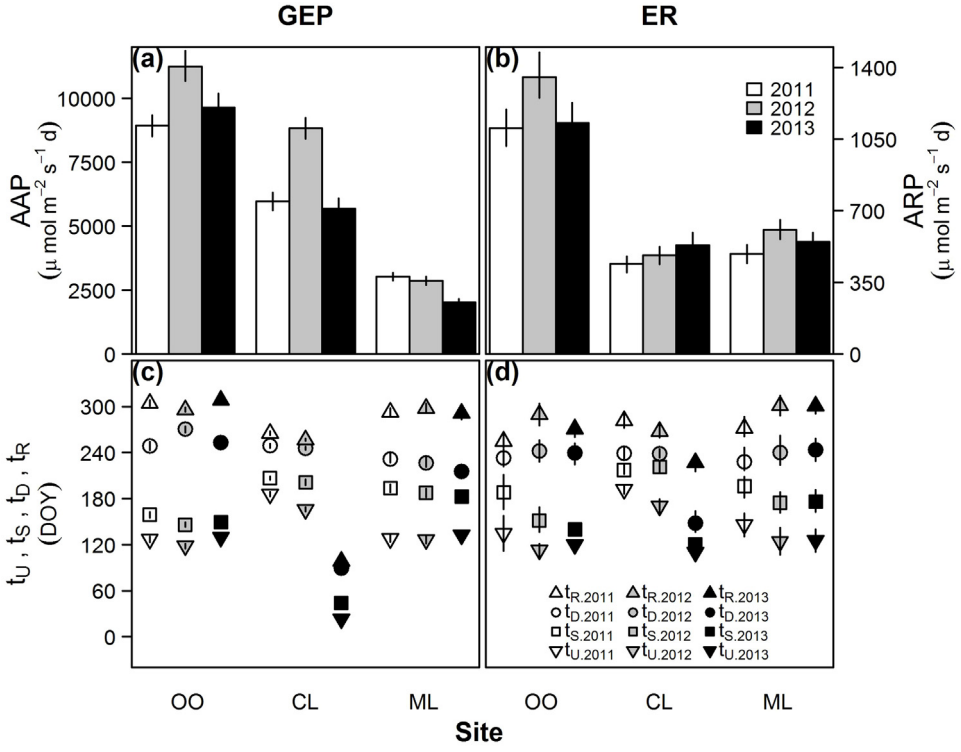

Fig. A3. Summary of the phenological indices at the woodland (OO), cropland (CL) and marsh (ML) sites, including (a) the annual assimilation potential (AAP), (b) annual respiration potential (ARP), (c) up-turn day (t_U), saturation day (t_S), down-turn day (t_D), and recession day (t_R) of the ecosystem CO_2 assimilation, and (d) t_U, t_S, t_D, and t_R of the ecosystem respiration. Data are presented as the year of 2011 (white), 2012 (gray), and 2013 (black). Vertical segments represent the 95% posterior quantile intervals. Detailed definition of these indices can be found in Gu et al. (2009).

Table A5
Model performance assessment for the half-hourly, daily, and eight-day F_{CO_2} at the woodland, marsh, and cropland sites.

Site	Year	Model statistics														
		Half-hourly[a]					Daily[b]					Eight-day[b]				
		N	β_0	β_1	R^2	MAE	*N*	β_0	β_1	R^2	MAE	*N*	β_0	β_1	R^2	MAE
Woodland	2011	7550	0.02	1.01	0.87	2.43	151	−0.01	1.05	0.98	0.36	24	−0.10	1.04	0.99	0.26
	2012	8018	0.05	1.01	0.93	1.98	172	0.10	1.01	0.98	0.35	25	0.06	1.00	0.99	0.22
	2013	7298	0.05	1.01	0.91	2.10	153	0.02	1.00	0.98	0.34	23	0.01	0.99	0.99	0.19
Cropland	2011	9630	0.05	1.01	0.93	1.23	208	0.10	1.01	0.98	0.19	34	0.13	0.98	0.99	0.13
	2012	10735	0.07	1.00	0.92	1.38	243	0.08	0.99	0.99	0.21	37	0.08	0.97	0.99	0.16
	2013	11450	0.04	1.02	0.93	1.38	266	0.06	1.01	0.99	0.19	41	0.08	1.01	0.99	0.15
Marsh	2011	12022	0.02	1.03	0.73	1.60	272	−0.02	0.99	0.98	0.17	38	−0.01	1.02	0.98	0.11
	2012	12643	0.01	1.01	0.81	1.08	302	0.00	1.01	0.97	0.15	41	0.00	1.02	0.99	0.09
	2013	13890	0.01	1.03	0.73	1.04	317	−0.02	1.04	0.96	0.13	46	−0.03	1.08	0.96	0.10

N, sample number; β_0, β_1, intercept and slope coefficients of linear regression; R^2, adjusted determination coefficient; MAE, mean absolute error.

[a] Half-hourly error statistics was obtained from the modeled and quality-controlled observed F_{CO_2} ($\mu mol\, CO_2\, m^{-2}\, s^{-1}$) ($F_{CO_2\cdot obs} \sim \beta_0 + \beta_1 \times F_{CO_2\cdot model}$).

[b] Daily and eight-day error statistics was obtained from the mean modeled and mean gap-filled F_{CO_2} ($g\, C\, m^{-2}\, d^{-1}$) for those periods that had less than 50% of gap-filled data ($F_{CO_2\cdot fill} \sim \beta_0 + \beta_1 \times F_{CO_2\cdot model}$).

treated independently and the unaccounted linkages among groups (e.g., among years, among seasons) often require extra works and caution in interpreting the modeling results.

The Bayesian hierarchical model takes advantage of linking the yearly parameters through higher level distributions (i.e., global) such that the year-to-year variation can be adequately described in the model structures and the overall estimate can be improved via sharing the information among years (Efron and Morris, 1977). Additionally, the seasonal and short-term (e.g., multi-daily or synoptic) dynamics of A_{max} and R_{ref} can be adequately described by using the prescribed empirical functions and random error structures. In our preliminary tests, we ran an additional model estimation by setting A_{max} and R_{ref} as a random-walk process, where A_{max} and R_{ref} were allowed to vary everyday through the

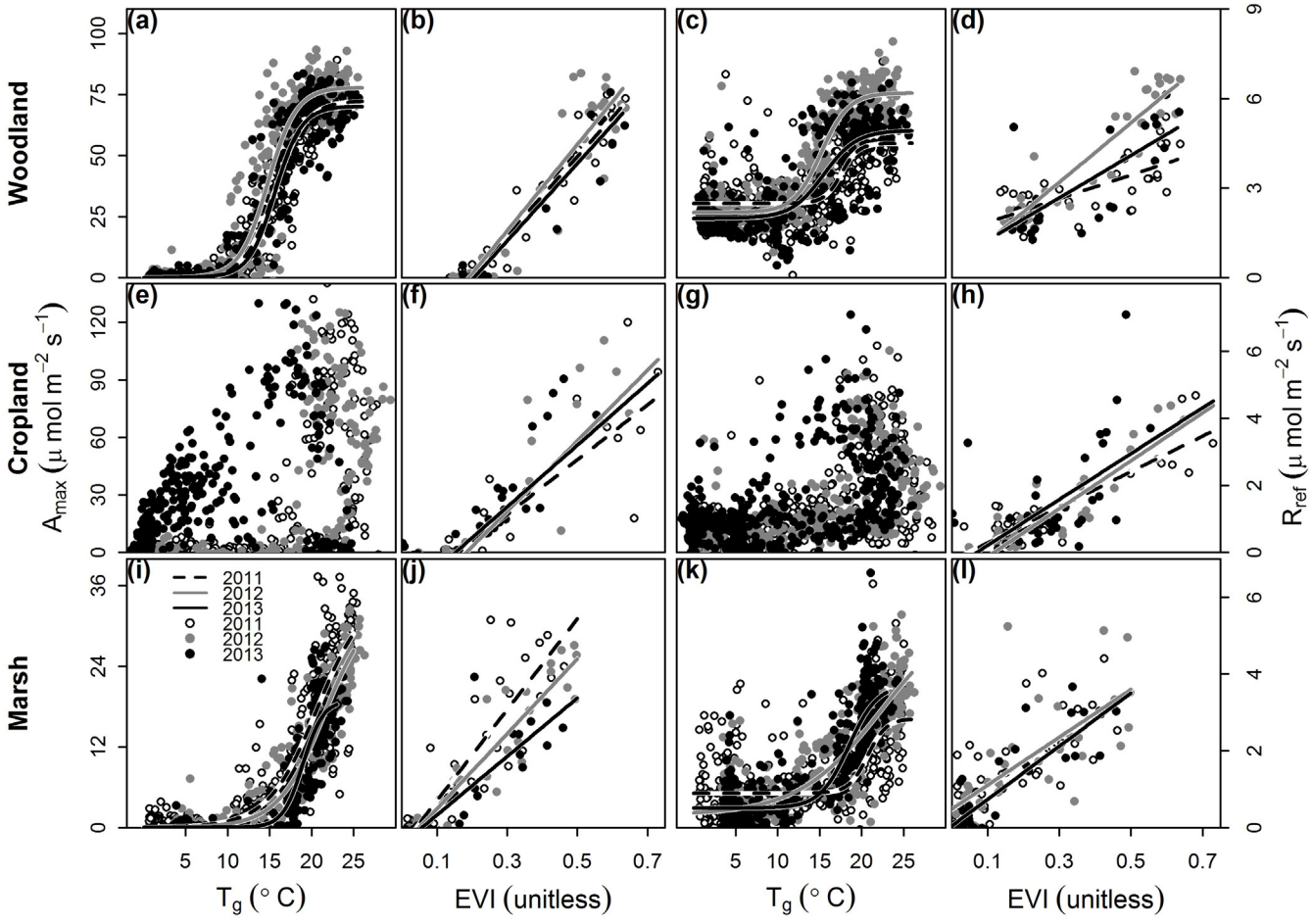

Fig. A4. The relationships of daily (a–b, e–f, i–j) A_{max} and (c–d, g–h, k–l) R_{ref} against the soil temperature (T_g) and enhanced vegetation index (EVI). Eight day EVI was calculated from the reflectance (MOD09A1) obtained from the Moderate Resolution Imaging Spectroradiometer (MODIS) instrument. The spatial extent was $500 \times 500\, m^2$ at the marsh and cropland while $2500 \times 2500\, m^2$ at the woodland site. Separate sigmoidal curves ($y = \alpha_0 + \alpha_1/(1 + \exp(\alpha_2 - \alpha_3 \times T_g))$; α_0–α_3 are model coefficients) are fitted to R_{ref} and A_{max} against T_g for each year at the woodland and marsh sites. Separate linear regressions are fitted to R_{ref} and A_{max} against EVI for each year.

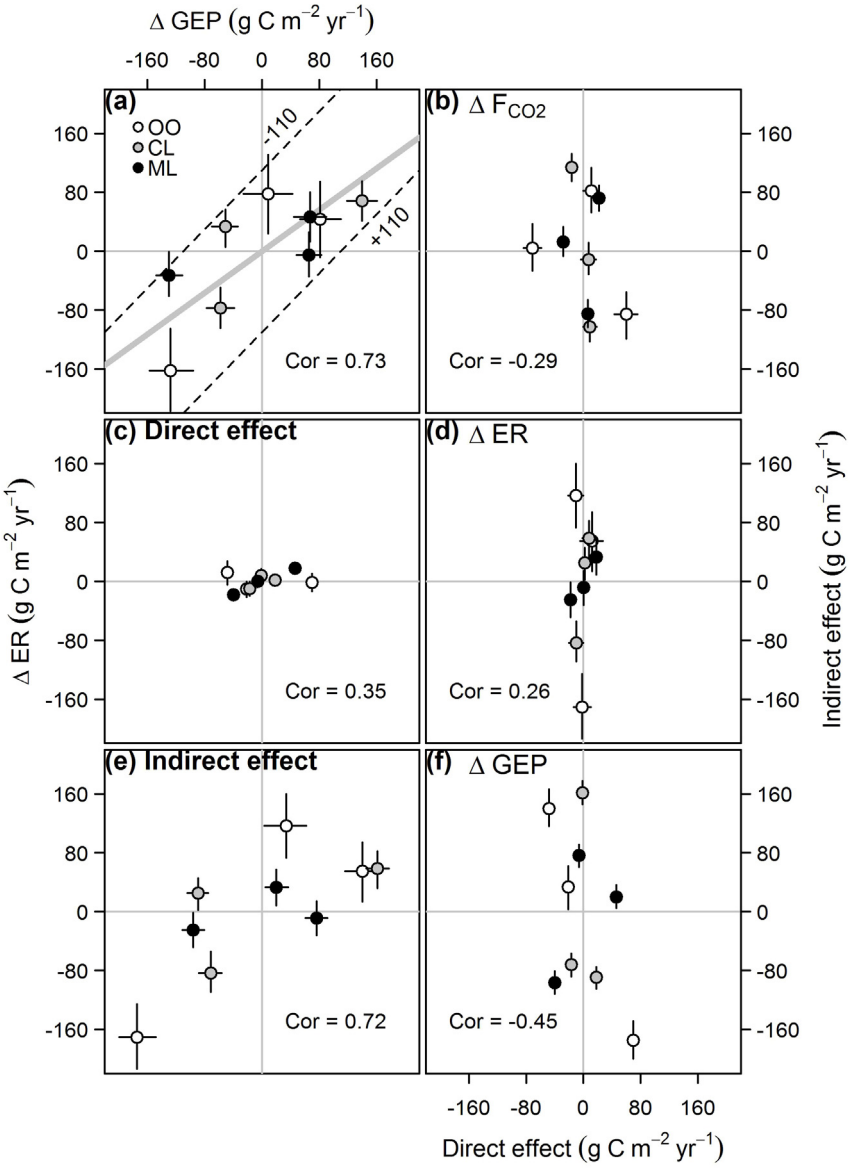

Fig. A5. Comparison of (a) the deviations, (c) direct effect, and (e) indirect effect of the annual gross ecosystem production (GEP) and ecosystem respiration (ER) among years and among sites. Comparison of the direct and indirect effects on interannual variability of (b) net ecosystem CO_2 exchange (F_{CO_2}), (c) ER, and (d) GEP. All deviations and effects were calculated based on the difference against the nine-scenario composite averages of each model at each site. White, gray, and black colors represent the woodland (OO), cropland (CL), and marsh (ML) sites, respectively. Vertical and horizontal segments indicate the 95% posterior quantile intervals. Dashed lines in Fig. A5a indicate the upper and lower bounds at which the year-to-year deviations of annual F_{CO_2} (i.e., $\Delta GEP - \Delta ER$) equal to $\pm 110\,g\,C\,m^{-2}\,yr^{-1}$. Gray solid line in Fig. A5a denote the pooled relationship ($\Delta ER = 0.704 \times \Delta GEP$) from the cross-site synthesis in Baldocchi (2008). Pearson correlations (Cor) are also calculated by using the data combined from all sites and all years.

time series while all other model structures were kept the same. We found that the random-walk model approach generated very similar seasonal and multi-daily dynamics in A_{max} and R_{ref} comparing to our current model (data not shown). This suggests that the current model structure was flexible and sufficient to capture the multi-scaled dynamics of CO_2 fluxes.

Second, the empirical phenological model we adopted provided an alternative approach in quantifying the GEP/ER phenology and thus in simulating the seasonality of CO_2 fluxes. Despite the fact that different equations were adopted, several previous studies have demonstrated that the phenological modeling approach was informative, practical, and flexible (e.g., Gu et al., 2003, 2009; Klosterman et al., 2014; Noormets et al., 2009; Toomey et al., 2015). Once these models were estimated, the first and second derivate could be calculated and a series of informative phenological indices could be determined along with properly-defined uncertainty intervals (e.g., Fig. A3). These mathematical characteristics make it feasible to draw statistical inference from the cross-site or cross-year comparison (Noormets et al., 2009).

It was also noticeable that most previous studies used daily maxima or integrals while fitting the phenological models (Gu et al., 2003, 2009; Noormets et al., 2009). We showed that our Bayesian hierarchical model could serve as an alternative approach in estimating the phenological indices. By using the half-hourly F_{CO_2} directly, such approach reduces the uncertainties that potentially originate from the gap-filling and/or GEP-ER partitioning procedures. Also, the short-term effects of environmental forcing, such as PAR/VPD on GEP and T_a/VWC on ER, can be explicitly incorporated into models. This helps eliminate the effects of short-term environmental forcing and provides better estimates of the potential GEP and ER.

References

Ault, T., et al., 2013. The false spring of 2012, earliest in north American record. EOS Trans. Am. Geophys. Union 94 (20), 181–182.

Baldocchi, D.D., et al., 2001. A spectral analysis of biosphere-atmosphere trace gas flux densities and meteorological variables across hour to multi-year time scales. Agric. For. Meteorol. 107 (1), 1–27.

Baldocchi, D.D., et al., 2005. Predicting the onset of net carbon uptake by deciduous forests with soil temperature and climate data: a synthesis of FLUXNET data. Int. J. Biometeorol. 49 (6), 377–387.

Baldocchi, D.D., 2008. Turner review No. 15. 'Breathing' of the terrestrial biosphere: lessons learned from a global network of carbon dioxide flux measurement systems. Aust. J. Bot. 56 (1), 1–26.

Baldocchi, D.D., 2014. Measuring fluxes of trace gases and energy between ecosystems and the atmosphere—the state and future of the eddy covariance method. Global Change Biol. 20, 3600–3609.

Barr, A.G., et al., 2004. Inter-annual variability in the leaf area index of a boreal aspen-hazelnut forest in relation to net ecosystem production. Agric. For. Meteorol. 126 (3), 237–255.

Barr, A.G., et al., 2009. Climate and phenological controls of the carbon and energy balances of three contrasting boreal forest ecosystems in western Canada. In: Noormets, A. (Ed.), Phenology of Ecosystem Processes: Applications in Global Change Research. Springer, New York, USA, pp. 3–34.

Black, T., et al., 2000. Increased carbon sequestration by a boreal deciduous forest in years with a warm spring. Geophys. Res. Lett. 27 (9), 1271–1274.

Bloom, A.A., Williams, M., 2015. Constraining ecosystem carbon dynamics in a data-limited world: integrating ecological "common sense" in a model – data fusion framework. Biogeosciences 12 (5), 1299–1315.

Braswell, B., et al., 1997. The response of global terrestrial ecosystems to interannual temperature variability. Science 278 (5339), 870–873.

Brooks, S.P., Gelman, A., 1998. General methods for monitoring convergence of iterative simulations. J. Comput. Graph. Stat. 7 (4), 434–455.

Carbone, M.S., et al., 2008. Soil respiration in perennial grass and shrub ecosystems: linking environmental controls with plant and microbial sources on seasonal and diel timescales. J. Geophys. Res.: Biogeosci. 113 (G2), G02022.

Chu, H., et al., 2014. Net ecosystem methane and carbon dioxide exchanges in a Lake Erie coastal marsh and a nearby cropland. J. Geophys. Res.: Biogeosci. 119 (5), 722–740.

Chu, H., et al., 2015. Climatic variability, hydrologic anomaly, and methane emission can turn productive freshwater marshes into net carbon sources. Global Change Biol. 21 (3), 1165–1181.

Ciais, P., et al., 2005. Europe-wide reduction in primary productivity caused by the heat and drought in 2003. Nature 437 (7058), 529–533.

Cook, B.D., et al., 2004. Carbon exchange and venting anomalies in an upland deciduous forest in northern Wisconsin, USA. Agric. For. Meteorol. 126 (3–4), 271–295.

Cox, P.M., et al., 2000. Acceleration of global warming due to carbon-cycle feedbacks in a coupled climate model. Nature 408 (6809), 184–187.

DeForest, J., et al., 2006. Phenophases alter the soil respiration–temperature relationship in an oak-dominated forest. Int. J. Biometeorol. 51 (2), 135–144.

DeForest, J., et al., 2009. Leaf litter is an important mediator of soil respiration in an oak-dominated forest. Int. J. Biometeorol. 53 (2), 127–134.

Desai, A.R., 2010. Climatic and phenological controls on coherent regional interannual variability of carbon dioxide flux in a heterogeneous landscape. J. Geophys. Res.: Biogeosci. 115 (G3), G00J02.

Desai, A.R., 2014. Influence and predictive capacity of climate anomalies on daily to decadal extremes in canopy photosynthesis. Photosynth. Res. 119 (1–2), 31–47.

Efron, B., Morris, C.N., 1977. Stein's paradox in statistics. Sci. Am. 236 (5), 119–127.

Falge, E., et al., 2001. Gap filling strategies for defensible annual sums of net ecosystem exchange. Agric. For. Meteorol. 107 (1), 43–69.

Gouhier, T., 2014. biwavelet: Conduct univariate and bivariate wavelet analyses (Version 0.14).

Grinsted, A., et al., 2004. Application of the cross wavelet transform and wavelet coherence to geophysical time series. Nonlinear Process. Geophys. 11, 561–566.

Gu, L., et al., 2003. Phenology of vegetation photosynthesis. In: Schwartz, M.D. (Ed.), Phenology: An Integrative Environmental Science. Tasks for Vegetation Science. Kluwer Academic Publishers, Netherlands, pp. 467–485.

Gu, L., et al., 2009. Characterizing the seasonal dynamics of plant community photosynthesis across a range of vegetation types. In: Noormets, A. (Ed.), Phenology of Ecosystem Processes: Applications in Global Change Research. Springer, New York, USA, pp. 35–58.

Heimann, M., Reichstein, M., 2008. Terrestrial ecosystem carbon dynamics and climate feedbacks. Nature 451 (7176), 289–292.

Hu, J., et al., 2010. Longer growing seasons lead to less carbon sequestration by a subalpine forest. Global Change Biol. 16 (2), 771–783.

Hui, D., et al., 2003. Partitioning interannual variability in net ecosystem exchange between climatic variability and functional change. Tree Physiol. 23 (7), 433–442.

Humphreys, E.R., Lafleur, P.M., 2011. Does earlier snowmelt lead to greater CO_2 sequestration in two low Arctic tundra ecosystems? Geophys. Res. Lett. 38 (9), L09703.

Jarvis, P., et al., 2007. Drying and wetting of Mediterranean soils stimulates decomposition and carbon dioxide emission: the "Birch effect". Tree Physiol. 27 (7), 929–940.

Karl, T.R., et al., 2012. U.S. temperature and drought: recent anomalies and trends. EOS Trans. Am. Geophys. Union 93 (47), 473.

Klosterman, S.T., et al., 2014. Evaluating remote sensing of deciduous forest phenology at multiple spatial scales using PhenoCam imagery. Biogeosciences 11 (16), 4305–4320.

Knudson, W.A., 2012. The Economic Impact of the This Spring's Weather on the Fruit and Vegetable Sectors. The Strategyic Marketing Institute, Michigan State University, East Lansing, MI, USA.

Kross, A.S.E., et al., 2014. Phenology and its role in carbon dioxide exchange processes in northern peatlands. J. Geophys. Res.: Biogeosci. 119 (7), 1370–1384.

Lafleur, P.M., et al., 2003. Interannual variability in the peatland-atmosphere carbon dioxide exchange at an ombrotrophic bog. Global Biogeochem. Cycles 17 (2), 1036.

Lafleur, P.M., Humphreys, E.R., 2008. Spring warming and carbon dioxide exchange over low Arctic tundra in central Canada. Global Change Biol. 14 (4), 740–756.

Lasslop, G., et al., 2010. Separation of net ecosystem exchange into assimilation and respiration using a light response curve approach: critical issues and global evaluation. Global Change Biol. 16 (1), 187–208.

Lloyd, J., Taylor, J.A., 1994. On the temperature dependence of soil respiration. Funct. Ecol. 8 (3), 315–323.

Luo, Y., et al., 2001. Acclimatization of soil respiration to warming in a tall grass prairie. Nature 413 (6856), 622–625.

Luo, Y., et al., 2009. Terrestrial carbon-cycle feedback to climate warming: experimental evidence on plant regulation and impacts of biofuel feedstock harvest. Global Change Biol.: Bioenergy 1 (1), 62–74.

McVeigh, P., et al., 2014. Meteorological and functional response partitioning to explain interannual variability of CO_2 exchange at an Irish Atlantic blanket bog. Agric. For. Meteorol. 194 (0), 8–19.

Melillo, J.M., et al. (Eds.), 2014. Climate Change Impacts in the United States: The Third National Climate Assessment. U.S. Global Change Research Program, Washington, DC, USA.

Moffat, A.M., et al., 2007. Comprehensive comparison of gap-filling techniques for eddy covariance net carbon fluxes. Agric. For. Meteorol. 147 (3–4), 209–232.

Morisette, J.T., et al., 2008. Tracking the rhythm of the seasons in the face of global change: phenological research in the 21st century. Front. Ecol. Environ. 7 (5), 253–260.

Noormets, A., et al., 2008a. Moisture sensitivity of ecosystem respiration: comparison of 14 forest ecosystems in the Upper Great Lakes Region, USA. Agric. For. Meteorol. 148 (2), 216–230.

Noormets, A., et al., 2008b. Drought during canopy development has lasting effect on annual carbon balance in a deciduous temperate forest. New Phytol. 179 (3), 818–828.

Noormets, A., et al., 2009. The phenology of gross ecosystem productivity and ecosystem respiration in temperate hardwood and conifer chronosequences. In: Noormets, A. (Ed.), Phenology of Ecosystem Processes: Applications in Global Change Research. Springer, New York, USA, pp. 59–85.

Ollinger, S., et al., 2008. Canopy nitrogen, carbon assimilation, and albedo in temperate and boreal forests: functional relations and potential climate feedbacks. Proc. Natl. Acad. Sci. 105 (49), 19336–19341.

Ouyang, Z., et al., 2014. Disentangling the confounding effects of PAR and air temperature on net ecosystem exchange at multiple time scales. Ecol. Complex. 19, 46–58.

Papale, D., et al., 2006. Towards a standardized processing of net ecosystem exchange measured with eddy covariance technique: algorithms and uncertainty estimation. Biogeosciences 3 (4), 571–583.

Plummer, M., 2003. JAGS: a program for analysis of Bayesian graphical models using Gibbs sampling. In: Hornik, K., et al. (Eds.), Proceedings of the 3rd International Workshop on Distributed Statistical Computing, Vienna, Austria.

Plummer, M., et al., 2006. CODA: convergence diagnosis and output analysis for MCMC. R News 6, 7–11.

Polley, H.W., et al., 2008. Interannual variability in carbon dioxide fluxes and flux-climate relationships on grazed and ungrazed northern mixed-grass prairie. Global Change Biol. 14 (7), 1620–1632.

Reichstein, M., et al., 2005. On the separation of net ecosystem exchange into assimilation and ecosystem respiration: review and improved algorithm. Global Change Biol. 11 (9), 1424–1439.

Richardson, A.D., et al., 2006. A multi-site analysis of random error in tower-based measurements of carbon and energy fluxes. Agric. For. Meteorol. 136 (1–2), 1–18.

Richardson, A.D., et al., 2007. Environmental variation is directly responsible for short- but not long-term variation in forest-atmosphere carbon exchange. Global Change Biol. 13 (4), 788–803.

Richardson, A.D., et al., 2009. Influence of spring phenology on seasonal and annual carbon balance in two contrasting New England forests. Tree Physiol. 29 (3), 321–331.

Richardson, A.D., et al., 2010. Influence of spring and autumn phenological transitions on forest ecosystem productivity. Philos. Trans. R. Soc. B: Biol. Sci. 365 (1555), 3227–3246.

Ryu, Y., et al., 2012. Continuous observation of tree leaf area index at ecosystem scale using upward-pointing digital cameras. Remote Sens. Environ. 126, 116–125.

Sala, A., et al., 2010. Physiological mechanisms of drought-induced tree mortality are far from being resolved. New Phytol. 186 (2), 274–281.

Shao, J., et al., 2014. Partitioning climatic and biotic effects on interannual variability of ecosystem carbon exchange in three ecosystems. Ecosystems 17 (7), 1186–1201.
Shao, J., et al., 2015. Biotic and climatic controls on interannual variability in carbon fluxes across terrestrial ecosystems. Agric. For. Meteorol. 205 (0), 11–22.
Shi, Z., et al., 2014. Differential effects of extreme drought on production and respiration: synthesis and modeling analysis. Biogeosciences 11 (3), 621–633.
Solymos, P., 2010. dclone: Data cloning in R. R Journal 2 (2), 29–37.
Soudani, K., et al., 2012. Ground-based Network of NDVI measurements for tracking temporal dynamics of canopy structure and vegetation phenology in different biomes. Remote Sens. Environ. 123 (0), 234–245.
Sowerby, A., et al., 2005. Microbial community changes in heathland soil communities along a geographical gradient: interaction with climate change manipulations. Soil Biol. Biochem. 37 (10), 1805–1813.
Stoy, P.C., et al., 2005. Variability in net ecosystem exchange from hourly to inter-annual time scales at adjacent pine and hardwood forests: a wavelet analysis. Tree Physiol. 25 (7), 887–902.
Stoy, P.C., et al., 2013. Evaluating the agreement between measurements and models of net ecosystem exchange at different times and timescales using wavelet coherence: an example using data from the North American Carbon Program Site-Level Interim Synthesis. Biogeosciences 10 (11), 6893–6909.
Sulman, B.N., et al., 2010. CO_2 fluxes at northern fens and bogs have opposite responses to inter-annual fluctuations in water table. Geophys. Res. Lett. 37 (19), L19702.
Teklemariam, T.A., et al., 2010. The direct and indirect effects of inter-annual meteorological variability on ecosystem carbon dioxide exchange at a temperate ombrotrophic bog. Agric. For. Meteorol. 150 (11), 1402–1411.
Thibault, K.M., Brown, J.H., 2008. Impact of an extreme climatic event on community assembly. Proc. Natl. Acad. Sci. U. S. A. 105 (9), 3410–3415.
Tierney, L., et al., 2009. Snow: a parallel computing framework for the R system. Int. J. Parallel Program. 37 (1), 78–90.
Toomey, M., et al., 2015. Greenness indices from digital cameras predict the timing and seasonal dynamics of canopy-scale photosynthesis. Ecol. Appl. 25 (1), 95–115.
Wu, J., et al., 2012. Effects of climate variability and functional changes on the interannual variation of the carbon balance in a temperate deciduous forest. Biogeosciences 9, 13–28.
Wuebbles, D.J., et al., 2014. Severe weather in United States under a changing climate. EOS Trans. Am. Geophys. Union 95 (18), 149–150.
Xiao, J., et al., 2010. A continuous measure of gross primary production for the conterminous United States derived from MODIS and AmeriFlux data. Remote Sens. Environ. 114 (3), 576–591.
Xie, J., et al., 2014. Long-term variability and environmental control of the carbon cycle in an oak-dominated temperate forest. For. Ecol. Manag. 313, 319–328.
Xu, J., et al., 2011. Influence of timber harvesting alternatives on forest soil respiration and its biophysical regulatory factors over a 5-year period in the Missouri Ozarks. Ecosystems 14 (8), 1310–1327.
Yi, C., et al., 2010. Climate control of terrestrial carbon exchange across biomes and continents. Environ. Res. Lett. 5 (3), 034007.
Zobitz, J., et al., 2011. A primer for data assimilation with ecological models using Markov Chain Monte Carlo (MCMC). Oecologia 167 (3), 599–611.